Master's Thesis of Science in Agriculture

A Study for Phenotype Analysis with the CRISPR Mediated Mice Model on the Skin Associated Immunity and Metabolism

CRISPR 유전자 적중 마우스 모델을 이용한 피부 면역 및 신진대사에 관한 표현형 해석 연구

August 2019

Ji Hyun Bae

Department of International Agricultural Technology

Graduate School of International Agricultural Technology

Seoul National University

A Study for Phenotype Analysis with the CRISPR Mediated Mice Model on the Skin Associated Immunity and Metabolism

A thesis
submitted in partial fulfillment of the requirements to the faculty
of Graduate School of International Agricultural Technology
for the Degree of Master of Science in Agriculture

By
Ji Hyun Bae

Supervised by
Prof. Su Cheong Yeom

Major of International Agricultural Technology
Department of International Agricultural Technology
Graduate School of International Agricultural Technology
Seoul National University

August 2019

Approved as a qualified thesis
for the Degree of Master of Science in Agriculture
by the committee members

Chairman	**Joong Hoon Park, Ph.D.**	_____
Member	**Tae Min Kim, Ph.D.**	_____
Member	**Su Cheong Yeom, DVM, Ph.D.**	_____

Abstract

A Study for Phenotype Analysis with the CRISPR Mediated Mice Model on the Skin Associated Immunity and Metabolism

Ji Hyun Bae

Department of International Agricultural Technology

The Graduate School of International Agricultural Technology

Seoul National University

Skin is the first barrier to body protection from injury and infection, one of the largest surface areas in the organs. Unlike the past, which is considered to be a simple physical barrier, recent studies have emphasized that skin is the front line organ of body homeostasis and actively contributes to the health of the body related to immunity or nonimmunity. To understand the functioning of these functions, it is necessary to observe the interactions and results of each sub-group that makes up the skin.

Most of the cellular functions of cells can be observed by simply modifying the genes associated with them. However, as mentioned above, the skin composed of various cell groups is a mutually important network. Therefore, it is advantageous to observe phenotypes in real-world environments through transgenic animal models as a result of interactions that may be lacking with In Vitro studies alone.

In this study, we examined the immunity of skin through CD80 CD86 gene mutation and the metabolic changes through Foxn1 gene mutation. Transgenic mice were constructed using the CRISPR / Cas system, which was proved to be an efficient and relatively simple genome editing tool.

The most important point in this study is that we can extract similar results as possible by analyzing phenotype considering complex and complex skin composition and function.

In conclusion, this study found a phenotype of hair loss and epidermal-associated metabolic changes associated with autoimmune diseases in the skin through the transformation of a single gene.

Keywords : Skin, Phenotype analysis, Gene editing, CD80CD86, Alopecia areata, Foxn1.

Student number : 2017-29998

Contents

Chapter II. Foxn1 is the regulator for thermogenic adipogenesis via keratinocyte.

List of Tables

List of Figures

Chapter I. CD80CD86 deficiency disrupts regulatory $CD4^+Foxp3^+$T cell homeostasis and induces autoimmune-like alopecia.

List of Figures

Chapter II. Foxn1 is the regulator for thermogenic adipogenesis via keratinocyte.

List of Abbreviations

Chapter I. CD80CD86 deficiency disrupts regulatory $CD4^{+}Foxp3^{+}$T cell homeostasis and induces autoimmune-like alopecia.

AA	**Alopecia areata**
ALA	**Autoimmune-like alopecia**
B6	**C57BL/6**
CD4	**Cluster of differentiation 4**
Foxp3	**Forkhead box P3**
H&E	**Haemotoxylin and Eosin stains**
hCG	**human chorionic gonadotropin**
IFN-γ	**Interferon gamma**
IHC	**Immunohistochemistry**
IL-4	**Interleukin 4**
MHC	**Major Histocompatibility complex**
PMSG	**Pregnant mare serum gonadotropin**
TCR	**T-cell receptor**
TGF-β1	**Transforming growth factor beta 1**
Th cells	**T helper cells**
Treg	**Regulatory T cell**

List of Abbreviations

Chapter II. Foxn1 is the regulator for thermogenic adipogenesis via keratinocyte.

BAT	**Brown adipose tissue**
BMP	**Bone morphogenetic proteins**
C/EBPa	**CCAAT/enhancer binding protein, alpha**
eWAT	**epididymal white adipose tissue**
FFA	**Free fatty acid**
Foxn1	**Forkhead box N1**
HDL	**High-density lipoprotein**
HFD	**High fat diet**
iWAT	**inguinal White adipose tissue**
NEFA	**Non-esterified fatty acids**
OGTT	**Oral glucose tolerance test**
PPARg	**Peroxisome proliferator-activated receptor gamma**
RER	**Respiratory exchange ratio**
scWAT	**subcutaneous White Adipose Tissue**
SNP	**Single nucleotide polymorphism**
TG	**Triglyceride**

Chapter I

CD80CD86 deficiency disrupts regulatory $CD4^{+}Foxp3^{+}$T cell homeostasis and induces autoimmune-like alopecia.

Introduction

Alopecia areata (AA) is an autoimmune disease associated with spot baldness in humans. Patients with AA exhibit non-scarring alopecia with a patchy, confluent, or diffuse pattern. Its incidence rate is similar in men and women, and the highest incidence of AA is observed in late childhood or early adulthood. Although the etiology of AA is not clear, it is known to be associated with genetic and environmental factors [1].

Autoreactive lymphocytic attack on the hair bulb may induce AA [2], and AA is often characterized by pigment incontinence and lymphocytic infiltration during the anagen or catagen stage of hair follicle growth [3]. Hair follicles exhibit immune privilege, with low MHC class I antigen expression, no MHC class II antigen expression, and strong transforming growth factor beta 1 (TGF-β1) expression [4]. When immune privilege of hair follicles collapses, interferon gamma (IFN-γ) expression and MHC class I antigen presentation occur on the hair follicle, and $CD4^+$ and $CD8^+$ T cells infiltrate into the

surrounding area [5, 6]. The balance between helper T (Th) cells and regulatory T cells (Tregs) is important in autoimmune diseases [7]. Indeed, in patients with AA, Treg function is decreased [8], and although the number of Tregs does not differ significantly, the inhibitory function of Tregs is impaired [9].

Animal models are essential for the study of autoimmune diseases. However, few models of AA have been developed. C3H/HeJ mouse strain is a well-known spontaneous AA mouse model. C3H/HeJ mice exhibit AA at an incidence rate of 0.035–0.25% at 5 months of age; however, this frequency increases up to 20% by 18 months of age [10]. C3H/HeJ mice with AA exhibit mononuclear cell infiltration during the anagen stage of the hair follicle growth, consistent with pathological signs of AA in humans. Immunologically, $CD4^+$ and $CD8^+$ T-cell infiltration and predominant Th1 cytokines are observed. Additionally, these mice show low levels of $CD4^+/CD25^+$ cells in the affected skin [11].

Recent studies indicate that CD28-CD80CD86 interaction is critically important for thymic selection and peripheral homeostasis of $CD4^{+}Foxp3^{+}$Treg cells [12, 13]. Moreover, CD80/CD86-knockout mice exhibit lower Treg populations than wild-type mice [14, 15]. Due to their distinct kinetics and affinities for the same receptor (CD28), it was suggested that whereas CD86 and CD80 contribute equally to thymic development of Tregs, CD86 is more important for peripheral homeostasis of Tregs than CD80 [16]. Therefore, I hypothesized that CD80CD86-deficient mice may exhibit symptoms of an autoimmune-like disease owing to the insufficient Treg population. Indeed, in my recent studies, I observed hair loss in

C57BL/6.CD80CD86-deficient mice, with mice having a macroscopic appearance similar to that observed in autoimmune alopecia. Accordingly, in this study, I characterized Treg populations and AA-related symptoms in CD80CD86-deficient mice to evaluate their applicability as a model of Autoimmune like-alopecia(ALA).

Material and Method

Mice

C57BL/6 (B6) and B6.129S4-CD80tm1ShrCD86tm2Shr/J (B6.CD80CD86$^{-/-}$) mice were purchased from Jackson Laboratory (Bar Harbor, ME). All mice in this study were maintained in individual ventilated cages under specific pathogen-free conditions and were given access to food and water ad libitum. This study was approved by the Institutional Animal Care and Use Committee of the Seoul National University and was conducted in accordance with approved guidelines.

Hair loss severity scoring

Hair loss severity scores were calculated by measuring the area of the affected skin, as previously reported with minor modifications [17]. Scores were assigned as follows: 0, normal; 1, less than 20% of the skin; 2, 20–40% of the skin; 3, 40–60% of the skin; and 4, more than 60% of the skin B6.CD80CD86$^{-/-}$ mice (n = 58) and B6 mice (n =40) were

analyzed at 34 weeks of age. Scoring was conducted by five different observers, and the significance of differences was analyzed. Additional scoring of hair loss was conducted with ImageJ program.

Histological analysis

For histological analysis, hematoxylin and eosin (H&E) staining of formalin-fixed tissues was conducted, and immunohistochemical staining was performed in 10-μm-thick optimum cutting temperature-fixed skin tissues from B6.CD80CD86$^{-/-}$ and B6 mice. Anti-mouse CD4, anti-Foxp3 (Santa Cruz Biotechnology Inc., Dallas, TX, USA), anti-mouse MHC class I and II (Abcam, Cambridge, MA, USA), and anti-CD8α (H-160; Biobyt, Berkeley, CA, USA) antibodies were used as primary antibodies. Biotinylated secondary antibodies and a Vectastain Elite ABC kit with diaminobenzidine (Vector Laboratories Inc., Burlingame, CA, USA) were used for detection. The comparison of Foxp3^{+} T cell numbers in the skin was conducted by counting positive cells from five different regions for each mouse (×400).

Flow cytometry analysis

Flow cytometry analysis was conducted in fresh splenocytes isolated from 4- and 30-week-old B6.CD80CD86$^{-/-}$ (n = 6) and B6 (n = 6) mice using a FACSCalibur cytometer (BD Bioscience, San Jose, CA, USA). Monoclonal antibodies targeting mouse Foxp3 (RJK-16), CD4 (RM4-5), CD8 (53-6.7), and CD25 (eBio7D4) were obtained from BD Bioscience.

Multiplex enzyme-linked immunosorbent assay (ELISA)

Concentrations of IFNγ, interleukin (IL)-2, IL-12, IL-4, IL-5, IL-10, and TGF-β1 were measured in the serum of 20–50-week-old B6.CD80CD86$^{-/-}$ (n = 8) and B6 mice (n = 7) with a multiplex sandwich immunoassay kit (Bio-Rad, Hercules, CA, USA) according to the manufacturer's instructions.

Quantitative polymerase chain reaction

Total RNA was extracted from the skin of B6 and B6.CD80CD86$^{-/-}$ mice using Trizol (Ambion). cDNA molecules were synthesized with a cDNA synthesis kit (ThermoFisher, MA, USA) according to the manufacturer's instructions. Quantitative RT-PCR was conducted with SYBR PCR premix (ThermoFisher) for IFN-γ and IL-12. All reactions were performed in quadruplicate, and gene expression levels were normalized to that of *Gapdh*. Primers of this study were obtained from the primer bank [18], and their sequences are provided in Supplementary Table 2.

CD25 inhibition test

Four groups of five B6 mice of both sexes were used for comparisons between young versus old animals. Six-week-old mice were used as the "young" group, and 8-month-old mice comprised the "old" group. Mice were randomly divided and injected intraperitoneally with 1 mg of anti-CD25 (clone PC-61.5.3; Bioxcell, West Lebanon, NH, USA) or control rat IgG (HRPN; Bioxcell) four times at biweekly intervals. After

the last anti-CD25 antibody injection, half of the mice were sacrificed for sample collection. The remaining mice were maintained for another four weeks without anti-CD25 antibody injections and sacrificed at 12 weeks after the first anti-CD25 antibody injection.

Statistical analysis

Statistical analysis was conducted by using the Student's t-test, Mann-Whitney U-test, and chi-squared test, as implemented in Prism 5.02 (GraphPad Software Inc., La Jolla, CA, USA)

Result

B6.CD80CD86$^{-/-}$ showed more severe hair loss than B6 mice.

I observed frequent occurrence of hair loss in B6.CD80CD86$^{-/-}$ mice. Female mice exhibited hair loss beginning at 8 weeks of age, and male mice exhibited hair loss beginning at 10 weeks of age. In both sexes, the onset of hair loss was similar in all animals kept in the same cage. Hair loss began in the neck area and extended to the dorsal part of the body trunk, but did not reach the ventral part of the body trunk. Hair loss became worse as mice aged, affecting almost the entire dorsal part of the body trunk at 3–4 months of age (Fig. 1A and Fig. S1A). Although some B6 mice also showed hair loss in the dorsal part of the body trunk, the prevalence and severity of this phenotype were significantly lower than in B6.CD80CD86$^{-/-}$ mice. The prevalence of hair loss calculated based on the appearance achieved 98% (56/57 mice) in 8-month-old B6.CD80CD86$^{-/-}$ mice, but only about 50% (20/40 mice) in B6 mice of the same age (Fig. 1B). Furthermore, the severity of hair loss was significantly higher in

B6.CD80CD86$^{-/-}$ mice than in B6 mice, as judged from score values (Fig. 1C). Further analysis of hair loss with ImageJ produced similar results as B6.CD80CD86$^{-/-}$ exhibited about 40–50% dimensional hair loss (Fig. 1D)

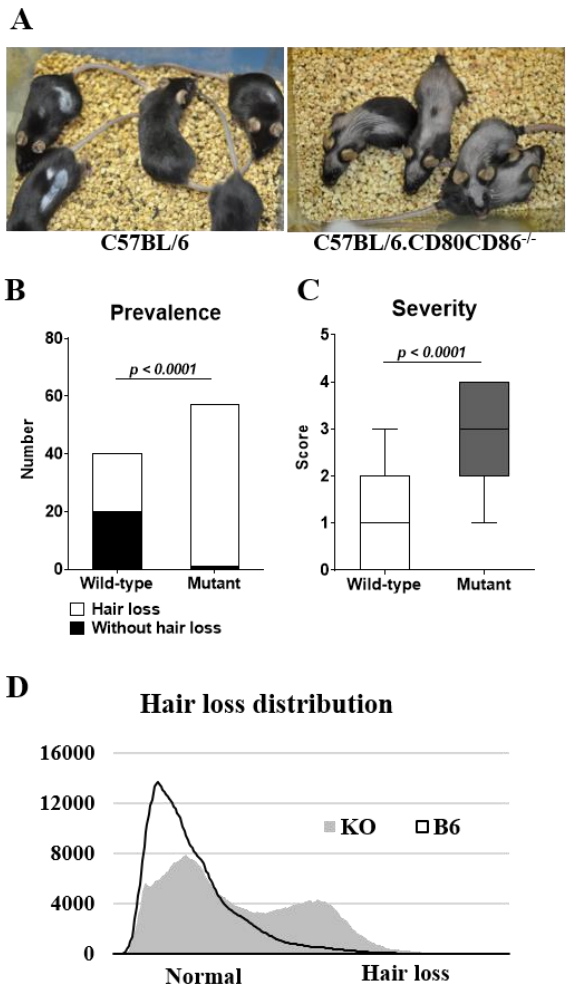

Figure 1. Hair loss in B6.CD80CD86$^{-/-}$ mice. A. Representative images of hair loss in 34-wk- old male B6 and B6.CD80CD86$^{-/-}$ mice. **B.** Incidence of hair loss was calculated based on the appearance: mice above grade 1 hair loss were regarded as affected at 34 wks. of age (B6; n=40, B6.CD80CD86−/−; n=58). P<.0001, chi- square test. **C.** Severity of hair loss is illustrated (B6; n=40, B6.CD80CD86$^{-/-,}$ n=58). P<.0001, Mann-Whitney U test. **D.** The area affected by hair loss was calculated by ImageJ software

Hair follicle destruction and T cell infiltration in the skin of B6.CD80CD86$^{-/-}$ mice.

H&E analysis of samples from 40-week-old B6.CD80CD86$^{-/-}$ mice revealed the occurrence of hair follicle destruction in the skin, but few remarkable lesions characteristic of an autoimmune-like disease in other organs (data not shown). Few differences in hair follicle destruction or histopathological changes were observed between male and female B6.CD80CD86$^{-/-}$ mice. Follicle destruction occurred in the hypodermis rather than in the dermis. I also observed coexistence of normal and damaged hair follicles, consistent with the diffuse-type hair loss in B6.CD80CD86$^{-/-}$ mice (Figs. 1A, 2, and S1B). However, B6 mice did not showed any remarkable histological changes, such as follicle destruction or broken hair in their spontaneous hair loss lesions.

Next, I used immunohistochemistry analysis to detect CD4^{+} and CD8^{+} T cells in 20-week-old B6.CD80CD86$^{-/-}$ mice. I observed typical T-cell infiltration: CD4^{+} T cells generally infiltrated the region around the terminal hair follicle, whereas CD8^{+} T cells infiltrated wider regions of the skin. In contrast, in B6 mice, no severe infiltration of

$CD4^+$ and $CD8^+$ T cells was observed. Indeed, MHC class I- and II-positive cells were observed in perifollicular region of B6.CD80CD86$^{-/-}$ mice. The location of $CD8^+$ and $CD4^+$ cells was similar to that of MHC class I and MHC class II molecules, respectively. There was no expression of MHC class I and II molecules in the hair follicle itself in B6.CD80CD86$^{-/-}$ mice. In accordance with the distribution of $CD4^+$ and $CD8^+$ T cells, hair follicles in B6 mice did not express MHC class I and II molecules (Fig. 2 and S2). These results suggested that hair loss in B6.CD80CD86$^{-/-}$ might have been caused by follicle destruction after T cell attack

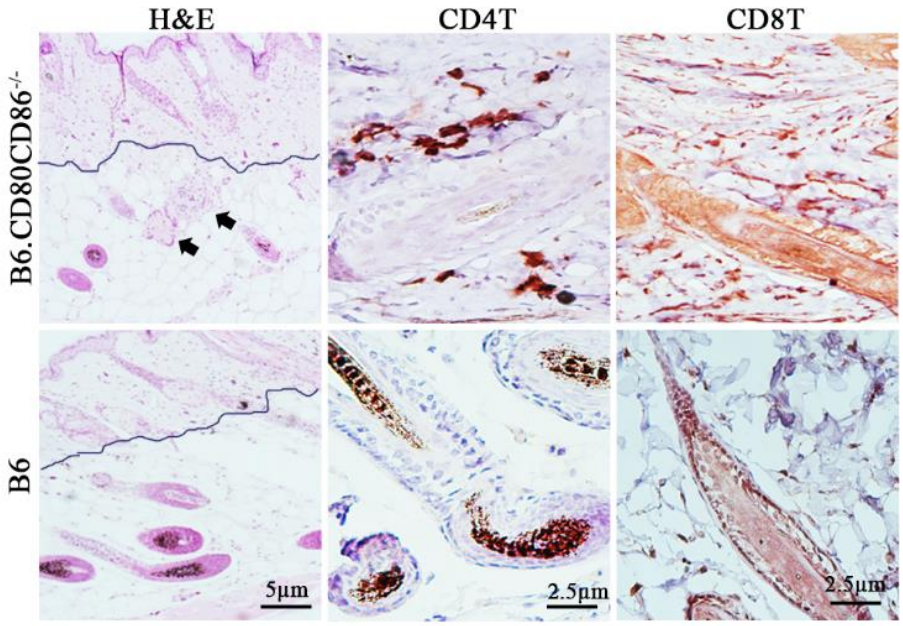

Figure 2. Histological examination of the skin in B6 and B6.CD80CD86−/−mice. Black arrow indicates the destruction of hair follicles (H&E, ×200, 40-wk- old B6 and B6.CD80CD86$^{-/-}$ mice). Immunohistochemical staining for CD4 and CD8 was conducted in samples from 10- to 20-wk-old male B6 and B6.CD80CD86$^{-/-}$ mice (×400)

Low $CD4^+CD25^+Foxp3^+$ Treg population in B6.CD80CD86$^{-/-}$ mice.

To confirm the role of T cells in causing hair loss in B6.CD80CD86$^{-/-}$ mice, immune cell kinetic analysis was performed in male B6 and B6.CD80CD86$^{-/-}$ animals. Flow cytometry analyses demonstrated that B6.CD80CD86$^{-/-}$ mice showed significantly lower frequency of $CD4^+Foxp3^+$ Treg cells than B6 mice (5.56% versus 21.00%; $P < 0.0001$, t test, Fig. 3A). Specifically, overall frequency of $CD4^+$ and $CD8^+$ T cells was not different between B6 and B6.CD80CD86$^{-/-}$ mice; however, the former showed a gradual increase in the number of $CD8^+$ T cells and $CD4^+CD25^+Foxp3^+$ Treg population with age. In B6.CD80CD86$^{-/-}$ mice, the frequency of $CD8^+$ T cells increased with age, whereas that of $CD4^+CD25^+Foxp3^+$ Treg cells did not change significantly between 4 and 30 weeks of age (Fig. 3B). Further analysis of absolute immune cell numbers revealed a similar pattern of immune cell frequency: B6 mice had a four- fold higher number of $CD4^+CD25^+Foxp3^+$ Treg cells than B6.CD80CD86$^{-/-}$ animals (Figs. S3A). Detailed information about the frequency and absolute numbers of immune cells is presented in Table S1.

Decreased Treg populations in B6.CD80CD86$^{-/-}$ mice were also detected during immunohistochemical analysis of skin samples. Foxp3^{+} Treg cells diffusely infiltrated in skin, and the total number of Foxp3^{+} Treg cells was significantly lower in B6.CD80CD86$^{-/-}$ mice than in B6 mice ($P = 0.02$, unpaired Student's t test, Fig. 3C and D). These results indicated that there was an imbalance of T cells and Treg cells in B6.CD80CD86$^{-/-}$ mice.

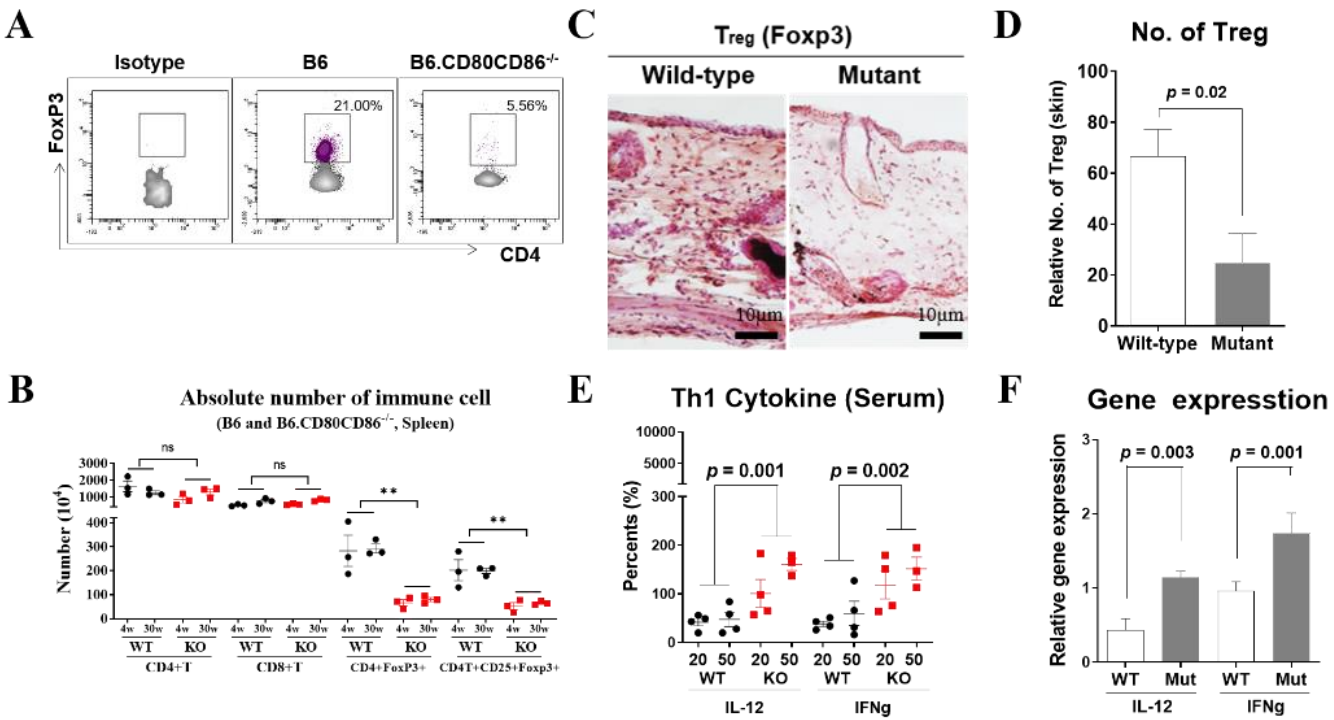
A
Isotype
B6
B6.CD80CD86-/-
FoxP3
CD4
21.00%
5.56%
C
Treg (Foxp3)
Wild-type
Mutant
10μm
10μm
D
No. of Treg
Relative No. of Treg (skin)
p = 0.02
Wilt-type
Mutant
B
Absolute number of immune cell
(B6 and B6.CD80CD86-/-, Spleen)
Number (10⁴)
ns
ns
**
**
4w 30w 4w 30w 4w 30w 4w 30w 4w 30w 4w 30w 4w 30w 4w 30w
WT KO WT KO WT KO WT KO
CD4+T
CD8+T
CD4+FoxP3+
CD4T+CD25+Foxp3+
E
Th1 Cytokine (Serum)
Percents (%)
p = 0.001
p = 0.002
20 50 20 50 20 50 20 50
WT KO WT KO
IL-12
IFNg
F
Gene expresstion
Relative gene expression
p = 0.003
p = 0.001
WT Mut WT Mut
IL-12
IFNg

Figure 3. Immune kinetics, cytokine concentration and immune-related gene expression analysis in B6 and B6.CD80CD86$^{-/-}$ mice. A. Percentage of CD4^{+} Foxp3^{+} Tregs in splenocytes of B6 and B6.CD80CD86$^{-/-}$ mice (n=5). **B.** Frequency of CD4^{+}, CD8^{+}, CD4^{+}Foxp3^{+} and CD4^{+}CD25^{+}Foxp3^{+} T cells in splenocytes of B6 and B6.CD80Cd86$^{-/-}$ mice. Each dot indicates a value from an individual mouse. Statistical analysis was conducted by the unpaired *t*-test. *Indicates significant difference (0.01<P<.05), and ** indicates very significant difference (0.01<P<.001). **C.** Immunohistochemical staining for Foxp3^{+} Tregs in the skin (100×). **D.** Numbers of Foxp3^{+} Tregs in five different tissues from each mouse (×400, 10-wk- old male B6 and B6.CD80CD86$^{-/-}$ mice). Statistical significance was calculated using the t test). **F.** Multiplex cytokine analysis was used to determine concentrations of IL- 12, IFNγ in 20- and 50-wk-old male B6 and B6.CD80C86$^{-/-}$ mice. Statistical analysis was conducted using unpaired t- test. Each dot indicates a value from an individual mouse. **G.** IL- 12 and IFNγ gene expression levels were analyzed by quantitative RT- PCR. Significance of differences (P<0.05) was calculated using the Student's unpaired *t*-test

High expression of Th1 inflammatory cytokine proteins and genes in B6.CD80CD86$^{-/-}$ mice.

Having documented lower number of $CD4^{+}CD25^{+}Foxp3^{+}$ Treg cells, I carried out additional analysis of systemic immune reactions by using multiplex ELISA. B6.CD80CD86$^{-/-}$ mice showed significantly higher serum concentrations of IL-12, IFNγ, IL-4, and IL-10 than B6 mice. In addition, concentrations of each cytokine in old mice were higher than in young mice. Furthermore, Th1-related cytokines, such as IL-12 and IFNγ, were secreted at higher concentrations by B6.CD80CD86$^{-/-}$ mice than by B6 animals (Fig. 3E and S3B).

Higher concentrations of inflammatory cytokines might represent a systemic immune response rather than a localized skin reaction, so additional quantitative RT-PCR was conducted using skin tissues. As shown in Fig. 3F, IL-12 and IFNγ gene expression levels were higher in tissues from B6.CD80CD86$^{-/-}$ mice, and this was consistent with the data on changes in cytokine proteins. These results suggested enhanced Th1 immune activation in B6.CD80CD86$^{-/-}$ mice.

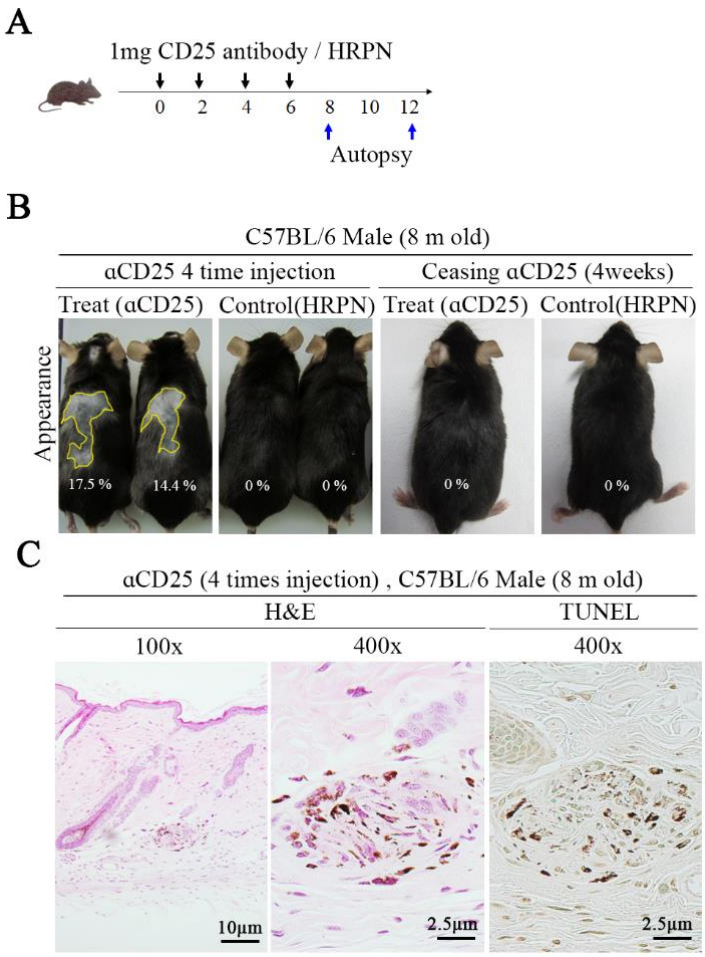

Figure 4. Effects of downregulation of CD25 in 8-mo-old B6 mice. A. Brief schematic representation of treatment of B6 and B6.CD80CD86$^{-/-}$ mice with an anti-CD25 antibody. Black arrows indicate anti- CD25 antibody injection, and blue arrows indicate euthanasia and autopsy. **B.** Gross appearance of skin samples from mice after treatment with an anti-CD25 antibody. **C.** Follicle destruction in an 8-mo- old male B6 mouse injected with an anti- CD25 antibody (H&E staining and TUNEL assay, ×100 and ×400 magnification levels, respectively).

CD25 depletion induced hair loss in old male B6 mice.

To confirm the role of Treg cells in the observed hair loss in B6.CD80CD86$^{-/-}$ mice, I performed CD25 depletion experiments in B6 wild-type mice. CD25 antibody injections induced partial depletion of CD4^{+}CD25^{+} Treg cell population. Furthermore, old male mice showed relatively higher depletion efficiency than did female mice (27% vs.17%, respectively; Fig. S4A and S4B).

Only old male mice treated with an anti-CD25 antibody showed mild hair loss with follicle destruction in the dorsal part of the body trunk. This effect was not observed in control mice treated with HRPN. Hair loss started at three weeks after the first antibody injection. H&E staining demonstrated that old B6 male mice treated with an anti-CD25 antibody exhibited damaged hair follicles similar to those observed in B6.CD80CD86$^{-/-}$ mice (Figs. 1A, 4B, 4C and S4C). Old female mice treated with an anti-CD25 antibody or HRPN showed only mild hair loss with skin redness on their back (Fig. S5A). In contrast to old male mice, old female mice treated with an anti-CD25 antibody did not show similar destruction of the follicular matrix. However,

mast cell infiltration was detected in both groups (Fig. S5B). Moreover, no young mice treated with an anti-CD25 antibody or HRPN showed hair loss or skin redness on macroscopic or microscopic examinations (Fig. S5C). Hair density recovered to normal in four weeks after the last CD25 antibody treatment in old B6 male and female mice. At that point, no damage to the follicular matrix was observed by microscopic analysis (Fig. S4C).

Discussion

The incidence of autoimmune diseases has continued to increase in recent decades. AA, an autoimmune disorder characterized by non-scarring reversible hair loss [1], is difficult to model in mice. The C3H mouse model is often used to study AA [10]. However, this model is limited due to the low incidence and late onset of symptoms relative to the time of peak AA incidence in humans, which occurs mainly during late childhood or early adulthood [10, 19]. In addition, other reported AA mouse models, such as A/J mice, also show late onset at 12–18 months of age [20]. Wild-type B6/J mice show high prevalence of hair loss co-occurring with ulcerative dermatitis during old age. Furthermore, vitamin A toxicity is known to cause hair loss in B6 mice [21]. These examples of hair loss in B6 mice do not represent autoimmune responses. In this study, I established B6.CD80CD86$^{-/-}$ mice, which showed etiopathogenesis similar to that observed in human AA, as a model to study ALA. Importantly, I observed severe

hair loss in B6.CD80CD86$^{-/-}$ mice and demonstrated that it was caused by the autoimmune response due to impaired Treg homeostasis.

In human AA, infection or stress can suppress the immune privilege of hair follicles, and complementary expression of autoantigens during the anagen stage of hair follicles can lead to the deposition of autoreactive CD4^{+} and CD8^{+} lymphocytes in the area, triggering an autoimmune response [22]. Even though MHC class I and II molecules were not expressed by the hair follicle itself, CD4^{+} T cell infiltration around the hair follicle was observed in B6.CD80CD86$^{-/-}$ mice. Additionally, CD8^{+} T cells were spread more diffusely than CD4^{+} T cells. Notable, all detected hair follicle destruction was observed in the hypodermal region of the skin. Mouse hair cycle is well characterized, and it is known that hair follicle matrix localizes to the hypodermal region during the anagen and catagen growth stages, and to the dermal region—during the telogen stage [23]. Thus, the destruction of terminal hair follicles in B6.CD80Cd86$^{-/-}$ mice appeared to occur during the anagen or catagen stages.

B6.CD80CD86$^{-/-}$ mice had significantly decreased Treg populations in the spleen and skin, consistent with data from previous studies in humans, which showed that CD80CD86 is important for maintaining homeostasis of CD4^{+} CD25^{+} Tregs [24]. CD80CD86 is a co-stimulatory factor for the T-cell receptor (TCR) that promotes the maturation of Treg precursors [25]. Intermediate or high TCR self-reactive thymocytes differentiate into Foxp3^{+} Tregs, whereas low TCR self-reactive thymocytes develop into Foxp3- naïve T cells or die by negative selection [26]. In relevance to our observations, CD80CD86-deficient NOD mice showed absence of Tregs [12], and the frequency of circulating CD4^{+} CD25^{high} Tregs was found to be significantly reduced or functionally impaired in human patients with autoimmune disease [27] and in C3H AA mice [11]. In addition, autoantigens from hair follicles stimulate Th1 and Tc cells; therefore, Th1 immune response is dominant in human AA. In our experiments, qPCR and multiplex cytokine analysis revealed enhanced Th1 immune activation in B6.CD80CD86$^{-/-}$ mice. CD80 and CD86 also have crucial roles in activation and differentiation of CD4^{+} and CD8^{+} T cell, so deficiency of these proteins in

B6.CD80CD86$^{-/-}$ mice could affect CD4^{+} and CD8^{+} T cell function [28]. However, there was little difference in CD4+ and CD8+ T cell population in B6 and B6.CD80CD86-/- mice, whereas clear hair loss pathogenesis was evident in the latter. A possible explanation to this discrepancy may be in the fact that CD4^{+}Foxp3^{+}Treg cells were dramatically decreased in the total CD4^{+} T cell population to the level of below 10% in secondary lymphoid organs. In this regard, I reasoned that pathological changes observed in CD80CD86$^{-/-}$ mice might be due to the imbalance of Tregs and self-reactive effector T cells. Therefore, I concluded that weak Treg function could not regulate over activation of effector T cells. In other words, hair loss in B6.CD80CD86$^{-/-}$ mice was caused by T-cell-mediated autoimmune-like response.

The important role of Tregs in hair loss was confirmed by experiments with B6 mice that underwent depletion of CD25-positive Tregs. Even though, CD25 is the alpha chain of IL-2 receptor and also expressed in activated T cell, but CD4^{+}Foxp3^{+}Treg cells express higher level of CD25 on their surface than activated T cell [29]. Thus CD25 antibody treatment preferentially affected and depleted CD25highFoxp3^{+} Tregs,

but not CD25low activated T effector cells in vivo [30]. The depletion of $CD4^+CD25^+$ cells was partial, and only old male mice showed hair loss with typical follicle destruction, which subsided following the cessation of the treatment. This suggested that even transient depletion of $CD25^+$ Tregs in peripheral blood can induce pronounced hair loss. This mechanism of this phenomenon is likely the imbalance between effector T cells and $Foxp3^+$ Tregs in the secondary lymphoid organ and disruption of peripheral tolerance. Although it is unclear why only old male mice showed this autoimmune-like response, the correlation between age and Treg function could explain this observation [31].

In summary, our findings demonstrated that B6.CD80CD86$^{-/-}$ mice showed impaired Treg homeostasis and developed autoimmune-related hair loss. Histologically, B6.CD8CD86$^{-/-}$ mice showed a low number of Tregs in the skin, high $CD4^+$ and $CD8^+$ T-cell infiltration around the terminal perifollicular region, and enhanced hair follicle destruction. I conclude that B6.CD80CD86$^{-/-}$ mice might have several advantages as a model of ALA, because they exhibited high incidence of disease-related phenotype,

early onset, and epipathogenesis similar to that observed in human AA. Thus, these mice could be utilized as a model of human autoimmune alopecia with pathological characterization.

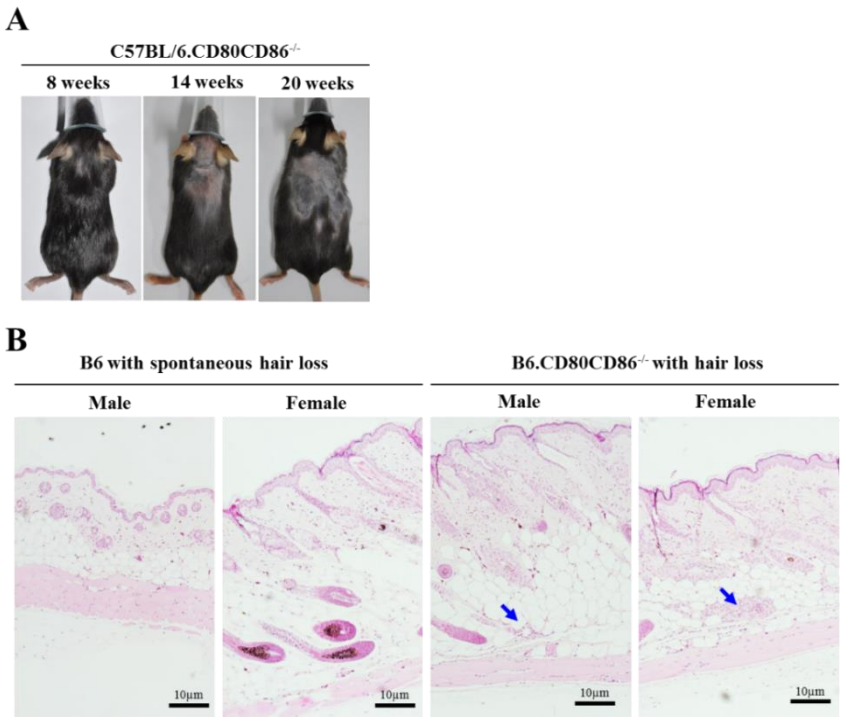

Supplementary Figure 1. Hair loss kinetics and histological examination. **A**) Hair loss kinetics in male B6.CD80CD86$^{-/-}$ mice from 8 to 20 weeks of age. **B)** Skin tissues were obtained from the hair loss region of 40 weeks old B6 and B6.CD80CD86$^{-/-}$ mice. Blue arrow indicate follicular destruction. (x100)

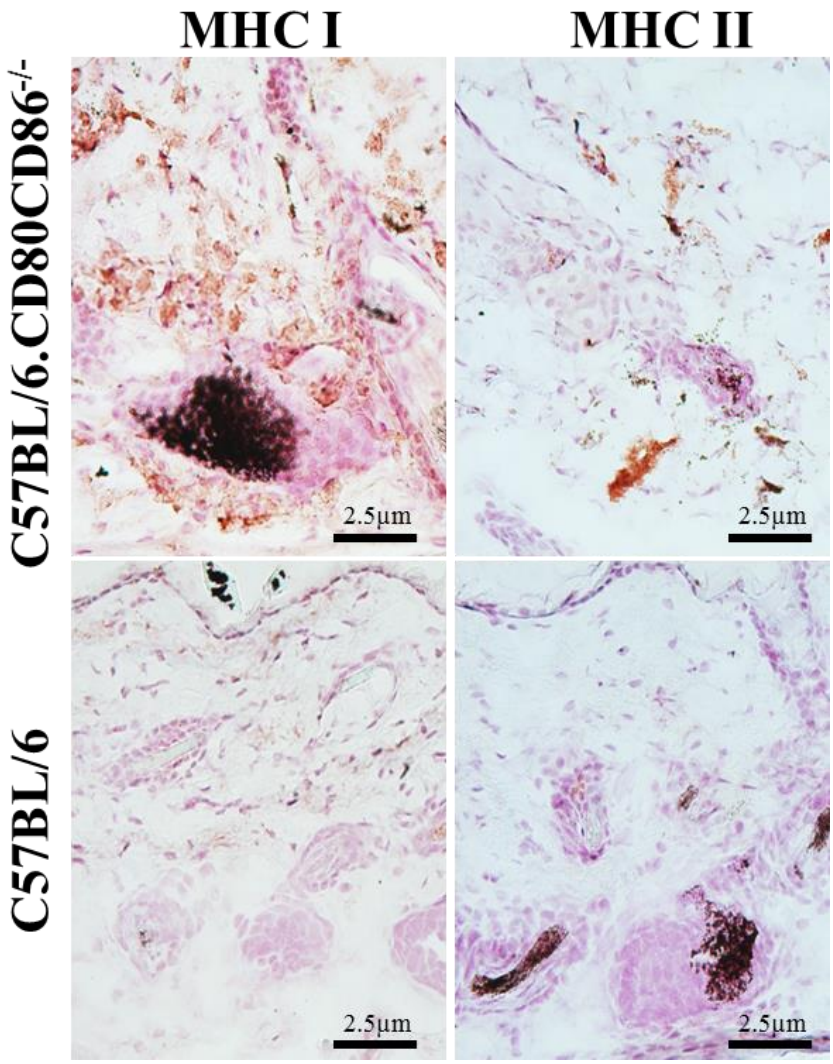

Supplementary Figure 2. Inmmunohistochemical staining for MHC class I and II molecules in sample from 10~20 weeks old male B6 and B6.CD80CD86$^{-/-}$ mice (x 400)

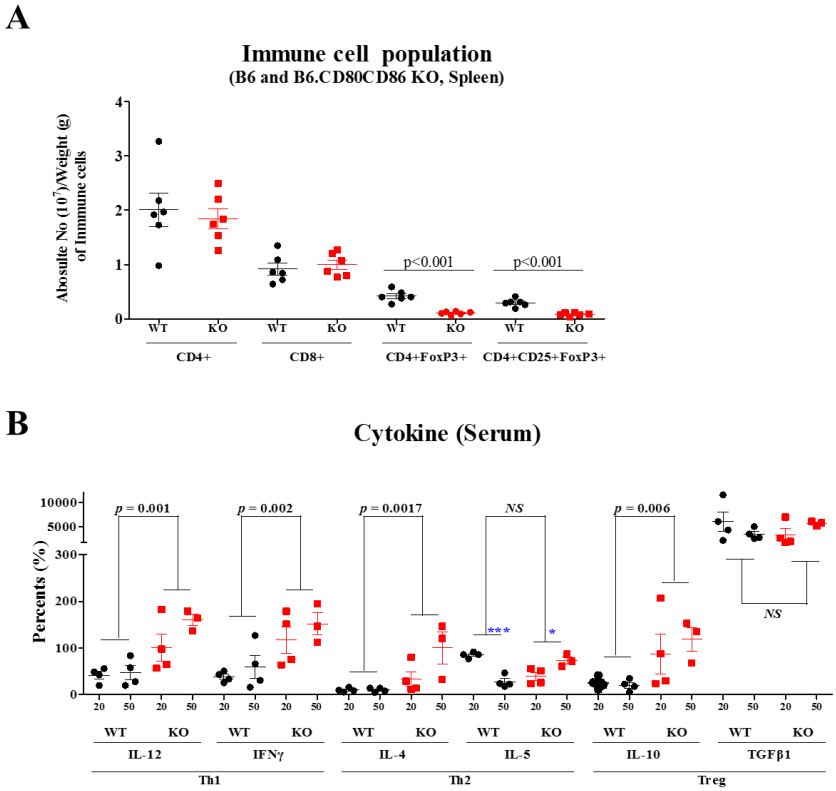

Supplementary Figure 3. Immune cell population and cytokine analysis in B6 and B6.CD80CD86-/-. **A**) Splenocytes from male B6 (n=6) and B6.CD80C86$^{-/-}$ mice (n=6) were analyzed with flowcytometry for CD4, CD8, CD25 and Foxp3. Absolute cell number of each immune cell were analyzed, statistical analysis was conducted with unpaired t test, and $p < 0.05$ mean significant difference. Detail information were in Supplementary Table 1. **B**) Multiplex cytokine analysis was used to determine concentrations of IL-12, IFNγ, IL-4, IL-10, IL-5, and TGF-β1 in 20- and 50-week-old male B6 and B6.CD80C86$^{-/-}$ mice. Statistical analysis was conducted by using unpaired *t*- test. Each dot indicates a value from an individual mouse. Data are represented as mean ± SEM.

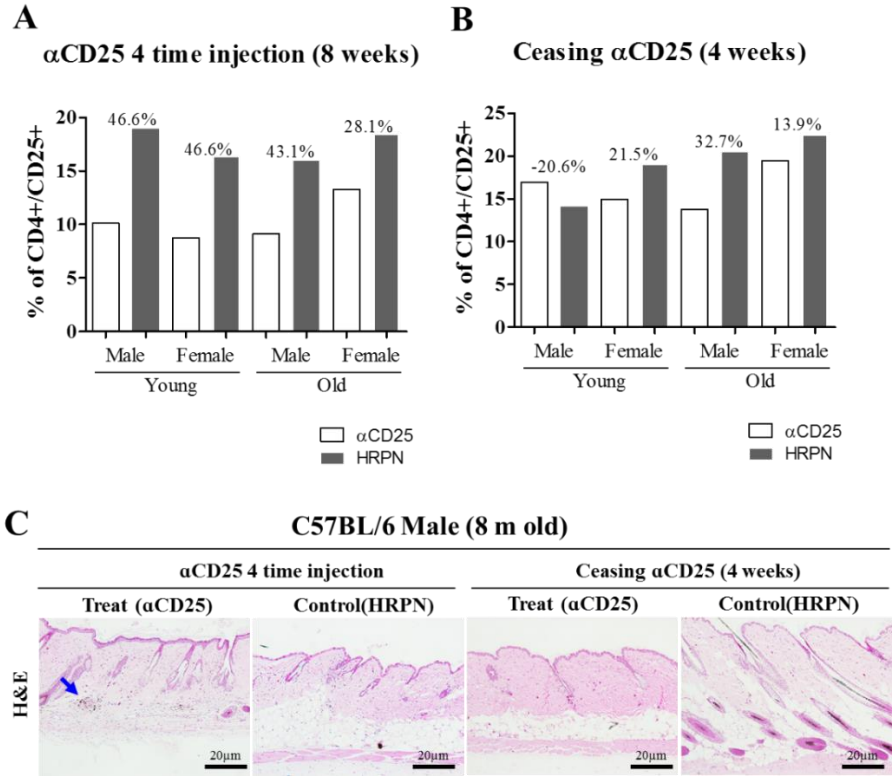

Supplementary Figure 4. Frequency of CD4CD25 positive splenocytes after CD25 antibody treated B6, and microscopic examination. A) After 8 weeks with 4 times anti CD25 antibody injection, all mice showed $CD4^{+}CD25^{+}$ Treg cell depletion than control mice, and old female mice showed relatively low depletion rate. **B**) The $CD4^{+}CD25^{+}$ Treg cell population was recovered after ceasing CD25 antibody treatment. Overall recovery rate was fast in young mice than old. Black numbers indicate gap of $CD4^{+}CD25^{+}$ Treg cell frequency between CD25 antibody treated and control group. **C)** H&E staining of skin samples from mice after treatment with an anti-CD25 antibody. Blue arrow in H&E indicates follicle destruction.

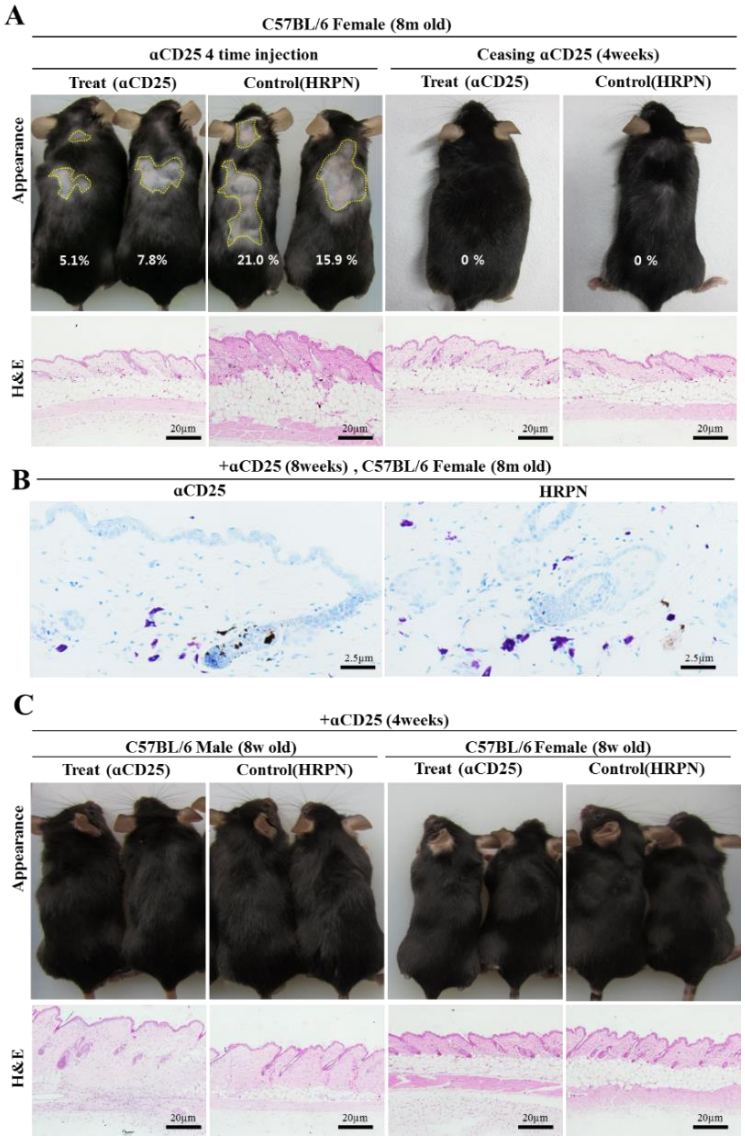

Supplementary Figure 5. Anti-**CD25 antibody treatment in B6.CD80CD86$^{-/-}$ and B6 mice. A)** Gross appearance and H&E of hair loss after CD25 antibody and HRPN treatment in 8 month old B6 female mice (100x). **B)** IHC for mast cells with toluidine blue stain (200×) in CD25 and isotype control treated mice. **C**) Gross appearance and H&E of hair loss after CD25 antibody and HRPN treatment in 8 weeks old male and female mice (100x)

Supplementary Table 1. Detail information about immune cell populations of B6 and B6.CD80CD86 knock mouse.

	Immune cell	B6 (male)		B6.CD80CD86 KO (male)	
		4 weeks old (n=3)	30 weeks old (n=3)	4 weeks old (n=3)	30 weeks old (n=3)
Percent (%)	CD4T	15.87	15.87	14.63	13.9
	CD8T	6.58	9.86	7.27	10.6
	CD4+Foxp3+	13.07	23.53	7.94	6.22
	CD4+CD25+Foxp3+	5.99	5.14	12.23	16.07
Absolute No. (10^4)	CD4T	1632	1250	836	1293
	CD8T	502	751	554	808
	CD4+Foxp3+	282.4	292.6	65.8	79.2
	CD4+CD25+Foxp3+	201.8	198.5	51.8	64.7
Absolute No. (10^4)/gram	CD4T	23890	16305	18576	18311
	CD8T	7360	11020	8128	11847
	CD4+Foxp3+	4140	4290	965	1162
	CD4+CD25+Foxp3+	2958	2910	759	948

Supplementary table 2. Specific primers for quantitative PCR

	Forward	Reverse	Size	Primer bank ID
IL12	ATGGCTGCTGCGTTGAGAA	AGCACTCATAGTCTGTCTTGGA	108	6680399a1
IFNg	TCCTCGCCAGACTCGTTTTC	GTCTTGGGTCATTGCTGGAAG	115	6680373a1

Chapter II

Foxn1 is the Regulator to Thermogenic Adipogenesis via Keratinocyte.

Introduction

Adipose tissue is an important part that regulates energy homeostasis by controlling size and number of adipocyte according to various conditions including nutritional status and temperature. While white adipose tissue stores excess energy, brown adipose tissue consumes energy in the form of heat production[32]. A beige adipose tissue (also called brite) represents an intermediate characteristic of both.

On the other hand, the metabolic abnormalities of obesity due to excessive energy accumulation are known to cause diabetes, heart disease or cancers. Obesity can be classified as visceral and subcutaneous according to the location of the fat accumulation, and it is known that each has different effects on the occurrence of metabolic abnormalities[33]. In particular, adverse effects associated with obesity are mainly caused by visceral adipose tissue, one of the representative white adipose tissue[34]. Ironically, brown adipocytes, which contain large amounts of mitochondria,

produce heat to repress the onset of hypothermia, obesity and diabetes. The relationship between the fat accumulation site and the adipocytes constituting it has been studied steadily, and the beige composition of subcutaneous white adipose tissue is attracting attention in recent years. beige adipocytes are an inducible form of thermogenic adipocytes that sporadically reside within WAT depots. Similar to brown adipocytes, beige adipocytes also possess abundant mitochondria. This beige adipocyte is a new target for the regulation of obesity and other metabolic disorders through the analysis of developmental processes and is expected to be a treatment for these diseases. But, the physiological significance of beige adipose tissue has not yet been fully explored. So, Expanding the understanding of beige adipocyte in subcutaneous will be of great help in the prevention and treatment of metabolic diseases.

The skin plays an important role in maintaining the homeostasis of the body, such as protection against external stimuli or maintenance of body temperature. Thus, the skin is composed of several different cell populations that are functionally different, and

epidermal keratinocytes are the most abundant type of cells. Complex interactions between keratinocytes and other cell populations are known to perform signaling functions in the skin and various tissues. Based on these characteristics, the skin has been studied for signal transduction with adipose tissue through factors associated with hair growth or differentiation [35,36]. However, the potential correlation between skin and scWAT remains unknown. In addition, the pathway for thermogenesis mediated beige adipose tissue in scWAT is still not clearly understood.

So, here I suggest that skin containing keratinocyte can affect the local accumulation of scWAT through the *Foxn1* gene mutated SNP mice. Down-regulation in signaling that originate from the skin, including the mutated gene, can have a significant impact on the association with adipose tissue and the subsequent understanding of metabolism.

Material and Method

Animal

All procedures related to mice were approved by the Institutional Animal Care and Use Committee guidelines of Seoul National University. C57BL/6 and ICR mice were purchased from a vender (Koatech, Korea). The mice were bred in our facility for laboratory animals under the SPF conditions with intervals of 12-hour dark cycle. All mice were maintained in individual ventilated cages and provided with pelleted foods and water ad libitum. In all experiments, only male animals were analyzed.

In vitro Oligonucleotides synthesis

pRGEN-dCas9-CMV/T7(H840A) and pRGEN-nCas9-CMV/T7(D10A) plasmids used as templates for mRNA transcription were obtained from Toolgen INC (Korea). The plasmids were linearized with XbaI and synthesized *in vitro* using the mMESSAGE mMACHINE T7 Ultra Transcription Kit (Thermo Fisher Scientific,

USA) according to the manufacturer's instruction. sgRNAs were designed according to its specific PAM sequence (NGG) and synthesized using a Megashortscript T7 Kit (Thermo Fisher Scientific, USA) through the PCR annealing of crRNA with T7 promotor and tracrRNA. CrRNA. The Cas9 mRNA and sgRNAs were purified with Megaclear Kit (Thermo Fisher Scientific, USA) and were prepared for microinjection.

Embryo preparation and Microinjection

C57BL/6 of the egg donor female were injected with 5 IU PMSG and hCG at 44-48 hour intervals for superovulation. On the following day, ovulated oocytes were collected and only fertilized zygotes were used for microinjection. Microinjection was conducted by micromanipulator (Eppendorf, Germany) for introducing site specific RNAs to zygote with two pronuclei. RNAs were provided in liquid form and each solution contained dCas9-mRNA(50ng/uL), nCas9-mRNA(50ng/uL) or sgRNA(10ng/uL). Embryos were cultured in vitro until the 2-cell stage and transferred to oviducts of surrogate ICR female mice.

Genotyping

Genomic DNA was extracted from the mice ear punches or toe tips of 2 weeks aged mice using a gDNA-extraction kit (Intron Bio, Korea) following manufacturer's instructions. The DNA was amplified by *AccuPower* Hotstart PCR PreMix (Bioneer, Korea) with primers containing a modified region of Foxn1gene [F: 5'-CTCTTCCCTTCTCTCCCT-3', R: 5'-TGTGACTTGGCCCTTCTG-3']. After PCR reaction, amplicons of each mouse were used for assay with T7 Endonuclease1(NEB, USA) and Sanger sequencing (Cosmo Genetech, Korea).

Experimental Diets, Weight, Food consumption and Body composition.

Each wild-type and C57BL/6.*Foxn1*$^{c.55C>A}$ mice were group housed in 4 or 5 mice per cage with wood chops for bedding. The experimental diets were compared using the standard laboratory chow and 45% High-Fat Diet (Research Diets Inc., USA). Each experimental group including mutant and wild-type mice were fed for 16 weeks from 5 weeks of age. The body weight and food intake were measured weekly during the

dietary regimen and parameters of body composition were analyzed using an InAlyzer (Medikors Inc., Korea) after 16 week diets. The parameters including body fat mass(g), lean mass(g), bone mineral content (%) and bone mineral density (%) were detected by x-ray absorption. To prevent movement, mice were anesthetized with isoflurane for scanning.

Sampling and H&E stain

eWAT, iWAT and iBAT of all mice were sacrificed to measure each mass after experimental diets. Some part of the harvested tissues, including skin, were stored with RNAlater at -80°C for RNA analysis. The other parts of skin, liver, eWAT, iWAT and iBAT were also fixed in 10% neutral formalin for 24 hours and embedded in paraffin for histological analysis. Paraffin-embedded tissues were sectioned 4μm, and were stained with hematoxylin and eosin following the standard protocol. Images of H&E stained tissue were acquired using CX23 microscope (Olympus, Japan) and were also

calculated to compare skin thickness. The number and size of adipocytes were analyzed using ImageJ (NIH, USA) software.

Energy Expenditure Measurement

Wild-type and mutant mice were housed individually in a PhenoMaster system (TSE-systems, Germany) for 5 Days after 11 weeks on the experimental diets. Not only was food consumption and water consumption recorded during this experiment, but Oxygen consumption (VO2), carbon dioxide production(VCO2), respiratory exchange ratio (RER = VCO2/VO2) and energy expenditure were calculated through the calibration system in this module.

OGTT, ITT and Biochemical analyses

The oral glucose tolerance tests (OGTT)s were performed after experimental diets. All mice were fasted overnight, and basal blood glucose level also were detected before administration of glucose (2g/kg) using Accu-chek glucose meter (Roche, Germany).

The glucose concentrations were continuously measured every 20 minute in the first 3 times, and then twice in 40 min intervals through the one droplet of blood from mice tail vein. For systemic insulin tolerance test, mice were fasted for 6 hours and were detected basal blood glucose level (0 minute). The blood glucose levels were analyzed in the same manner as described above after i.p. insulin injection (0.5U/kg).

Biochemical assays such as NEFA, TG, and HDL levels used in this study were performed using serum from mice tail vein. Non-esterified free fatty acids(NEFA) were detected using a NEFA-HR2 kit (Wako, Japan) according to the Mouse Metabolic Phenotyping Centers protocol (C1057). Concentrations of triglyceride (TG) and high-density lipoprotein cholesterol (HDL-cholesterol) were also measured using an enzyme-based kit (Asan, Korea) according to the manufacturer's instructions.

Gene expression analysis

For analysis of gene expression, total RNA was isolated from skin, epididymal White Adipose Tissue(eWAT) and inguinal White Adipose Tissue(iWAT) using trizol (Thermo fisher science, USA) according to the standard protocol, and was reverse transcribed by the High Capacity RNA to cDNA Kit (Applied Biosystems, USA) according to the manufacturer's instructions. Quantitative RT-PCR was conducted by StepOne Plus Real-time PCR system (Applied Biosystems, USA) with PowerUp SYBR Green Master Mix (Thermo Fisher Scientific, USA) under the following condition: 50 °C for 2 min, 95 °C for 2 min, 40 cycles of denaturation at 95 °C for 3sec, annealing and extension at 60 °C for 30sec. The Specificity of amplification was confirmed by melting curve detection at the end of each targets PCR reaction. The threshold cycle (Ct) values of each target were normalized by the Ct value of *Tbp* gene in order to compare the relative expression ratios between the experimental groups. The result was calculated with the $2^{-\Delta\Delta Ct}$ method. The sequences of primers were from the PrimerBank (https://pga.mgh.harvard.edu/primerbank/) listed in Table 1.

Statistical analysis

Statistical analysis was performed using the Graphpad Prism 8.1.1 (Graphpad software, USA) and data area presented as Mean±SEM. Differences were considered to be significant when *P*-value was less than 0.05.

Table 1. Specific primers for quantitative PCR

Gene	Forward	Reverse	Size	Primer bank ID
Foxn1	ATGGTGTCGCTACTCCCTCC	AGGCACAAACGACGAGCAG	108	6680211a1
Wnt10b	GAAGGGTAGTGGTGAGCAAGA	GGTTACAGCCACCCCATTCC	158	6756003a1
Wnt5b	CTGCTGACTGACGCCAACT	CCTGATACAACTGACACAGCTTT	145	6678599a1
Ctnnb1	ATGGAGCCGGACAGAAAAGC	CTTGCCACTCAGGGAAGGA	108	6671684a1
TCF	AGCTTTCTCCACTCTACGAACA	AATCCAGAGAGATCGGGGGTC	115	6678245a1
PPARg	TCGCTGATGCACTGCCTATG	GAGAGGTCCACAGAGCTGATT	103	6755138a1
C/EBPa	CAAGAACAGCAACGAGTACCG	GTCACTGGTCAACTCCAGCAC	124	6680916a1

.Results

Fonx1^{L19M} SNP mice generation with Cas9 base editing

Loss of function mutation in *Foxn1* gene developed hairless and athymia with severe immune deficiency phenotype[35], and there was studies about gene expression in skin and metabolic phenotype[36, 37]. However, hairless mice spent much energy for maintaining body temperature, thus they might not be appropriate for studying *Foxn1* gene function in metabolism[37]. Instead of gene knock out, small nucleotide alteration also change the its gene function or amount of gene expression[38]. Thus I tried to generate *Foxn1* mutant mice with harboring nucleotide substitution and without indels. Foxn1 is a transcription factor and participate skin epithelial cell proliferation[39], and its base-contacting residues are known as NH3-N47-S48-R50-H51-S54-L55-COOH in Forkhead domain[40]. In addition, Joseph et al[41] reported that, nucleotide deletion in 154 amino acid in the Foxn1 N-terminal also exhibited mild

thymus phenotype. In order to develop SNP close to start codon site, Cas9 base editing (Cas9-BE) technique was applied for mutant animal production[42]. First, SNP formation potential for Cas9-BE, I compared nCas9-BE and dCas9-BE using embryos. dCas9-BE presented only SNP without indel, but nCas9-BE developed SNP with indel formation (Figure 1a). Since, indel in exon would cause loss of function with premature stop codon formation, nCas9-BE mRNA and sgRNA were microinjection into pronucleus of mice one cell embryo. Among the obtained pups, two mice exhibited SNP as pL19M (cC55A) and pL19Q (cT56A), and pL19M mice exhibited obesity phenotype (Figure 1b).

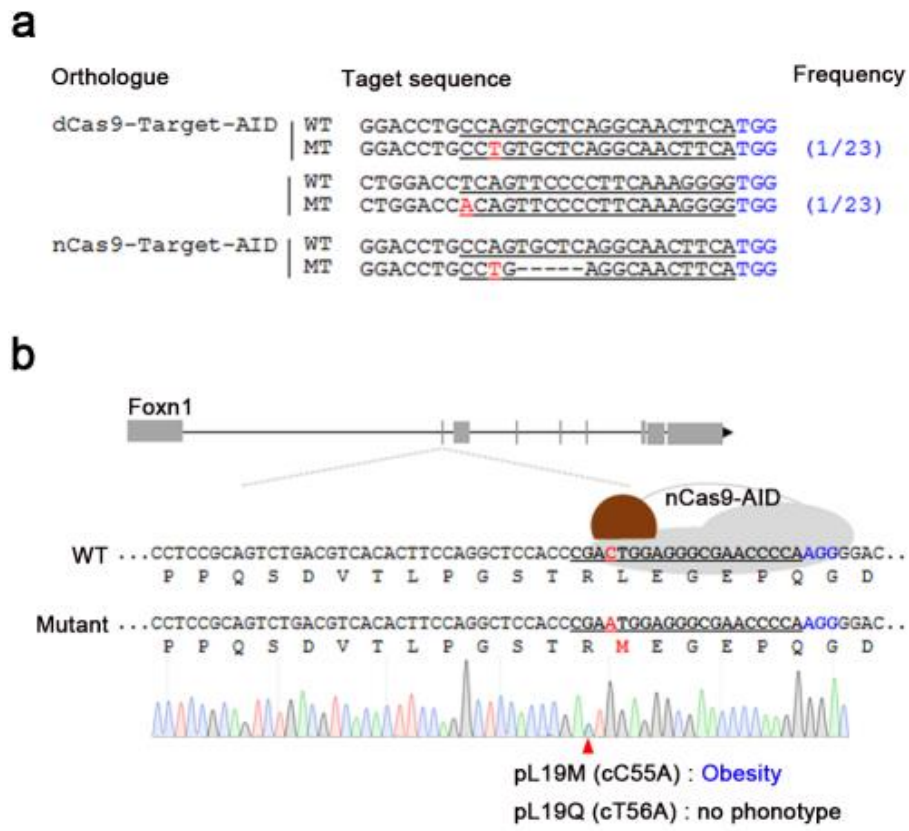

Figure 1. Generation of Foxn1^{L19M} mice with base editing. a. Nucleotide substitution or indel formation was assessed with microinjection into the mouse embryos. Two different CRISPR as nickage Cas9-BE and wild Cas9-BE was applied. Red alphabet: nucleotide substitution, -: deletion, blue alphabet: PAM sequence **b**. Gene editing strategy for base editing on N terminus of Foxn1 with nSpCas9-BE, and targeted sequence of founder mice. Red alphabet: nucleotide substitution.

Obesity with increasing subcutaneous fat mass but not lean mass on Foxn1^{L19M}

For further metabolic phenotype analysis for Foxn1^{L19M}, homozygote mutant mice were obtained with breeding, and subjected to 45% lipid containing high fat diet (HFD) and normal chow feeding experiment for 16 weeks. In normal chow feeding experiment, there was little difference on growth rate and feed consumption, but Foxn1^{L19M} mice showed increasing weight gaining than Foxn1^{WT} mice with similar amount of feed consumption. Male Foxn1^{L19M} mice exhibited higher weight discrepancy than female, and this might be caused with hormonal effect such as estrogen[43] (Figure 2a). Further analysis for body composition with Dexa-scan, normal chow did not affect fat and lean mass ratio, but HFD induced significant weight gaining only with fat mass increasing in Foxn1^{L19M} male mice (Figure 2b).

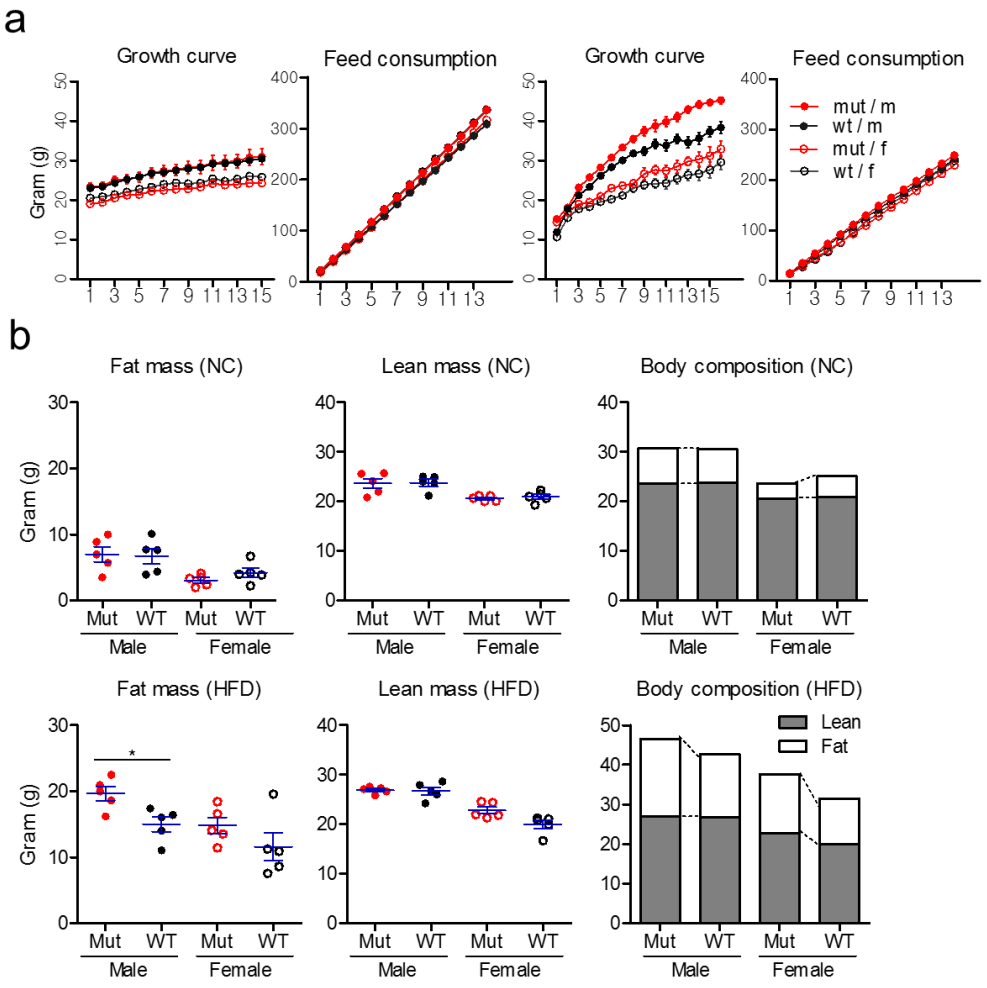

Figure 2. Obesity phenotyping of Foxn1^{L19M}.a. Growth and feed consumption analysis with normal chow and 45% high fat diet under 24 ℃ condition. (n=5) b. Dexa-scan based analysis for fat, lean mass. Spots indicate individual mice (n=5). Data are represented as mean ± SEM.

Increasing of subcutaneous fat in Foxn1^{L19M}

Next, I examined weight of each eWAT, iWAT and BAT of each mouse, and Foxn1^{L19M} mice induced fat mass increasing than Foxn1^{WT} mice except eWAT with HFD feeding (Figure 3a). In additional histological examination, Foxn1^{L19M} with normal chow (Foxn1$^{L19M\text{-}NC}$) feeding presented relatively larger adipocyte than Foxn1^{WT} mice with normal chow (Foxn1$^{WT\text{-}NC}$). Foxn1^{L19M} with HFD (Foxn1$^{L19M\text{-}HFD}$) developed peri-vascular steatosis in the liver, larger adipocyte in iWAT and more lipid deposition in BAT. There was crown-like structure in the eWAT from Foxn1$^{L19M\text{-}HFD}$, and this might be process of dying adipocyte and macrophage infiltration[44] (Figure 3b). Nevertheless, especially in HFD diet mice, increasing fat mass observed in the subcutaneous fat, and they were considered as thermogenic fat[45].

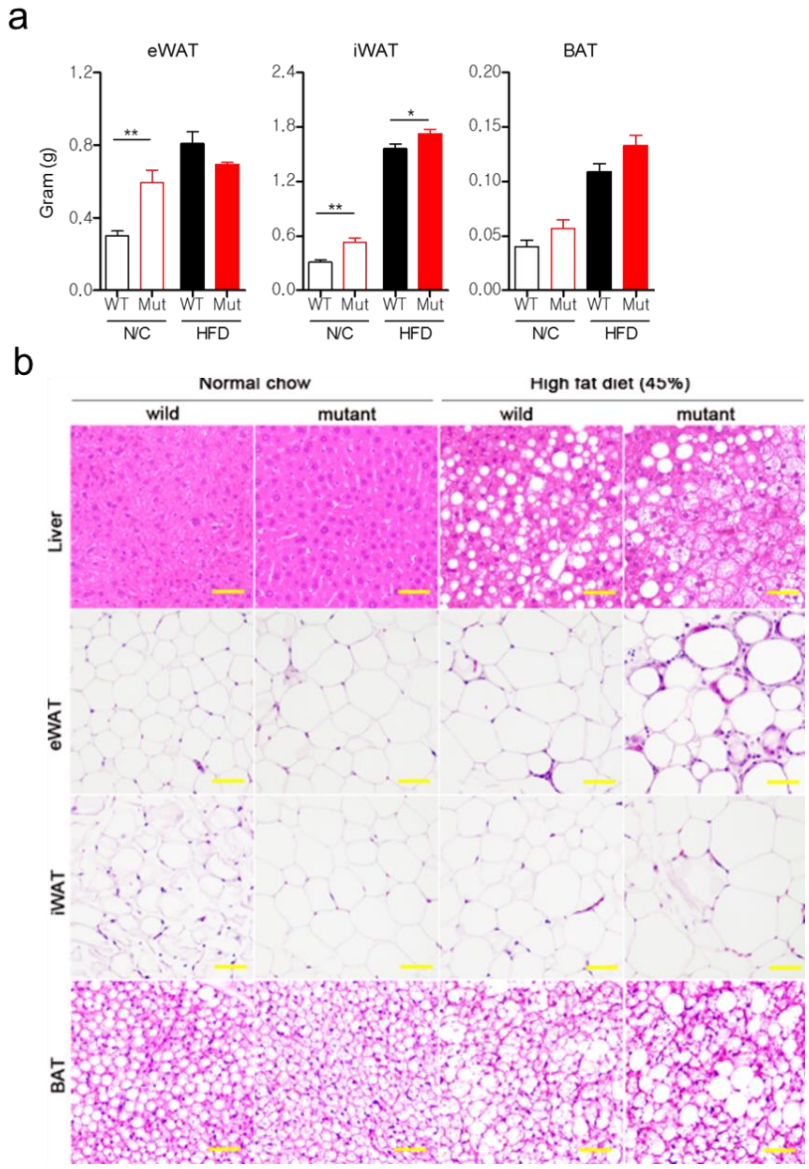

Figure 3. Histological analysis for iWAT, eWAT, BAT and liver. a. Weight of eWAT, iWAT and BAT was measured and compared. * indicate significant of $p < 0.05$ **b**. H&E staining for liver, eWAT, iWAT and BAT. Yellow bar: 100 μm

iWAT was normally analyzed fat site which is represent subcutaneous and beige character, but there was little report analyzing subcutaneous fat on hypodermis, thus addition microscopic analysis for skin fat was conducted. In microscopic examination on skin tissues, thickness of subcutaneous fat was significantly increased as approximate 34% in normal chow, and 92% in HFD (299.3 ± 19.5 vs 403.5 ± 18.8 μm in normal chow and 488.7 ± 18.4 vs 941.9 ± 68.7 μm in HFD). The subcutaneous fat thickening caused by adipocyte hyperplasia and hypertrophy (Figure 4a). Recently, Giacomo et[46] al reported that subcutaneous fat adipogenesis was controlled by keratinocyte derived wnt/β-catenin signaling depending on hair follicle growth cycle, but there was litter histological difference in dermis and hair cycle between $Foxn1^{L19M}$ and $Foxn1^{WT}$ mice (Figure 4b).

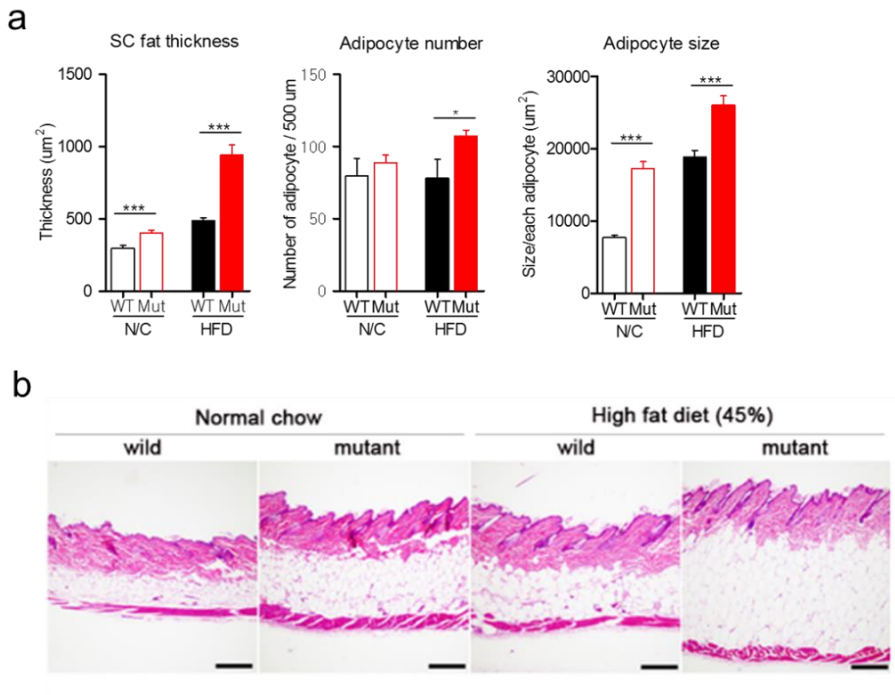

Figure 4. Histological analysis for subcutaneous fat. a. Comparison subcutaneous fat thickness (10 different site, μm) and adipocyte numbers and adipocyte size within 500μm width. *: $p < 0.05$. ***: $p < 0.0001$ in unpaired student *t* test. **b.** H&E staining for skin tissues from Foxn1^{L19M} and Foxn1^{WT} mice with normal chow and HFD diet. Representative image is presented. Black bar: 500 μm.

High activity but low energy expenditure in Foxn1^{L19M}

After confirming high thermogenic adipogenesis on Foxn1^{L19M}, metabolic phenotype was analyzed with PhenoMaster. Feed consumption is almost similar with Foxn1^{L19M} and Foxn1^{WT} mice, but Foxn1^{L19M} drink more water than Foxn1^{WT} mice in the HFD diet group. Interestingly, gap of water consumption happened in night, but the reason and influence for polydipsia is still uncertain. In the activity analysis, mice showed high activity in night, and mice with normal chow was more active than HFD group (Figure 5a). Foxn1^{WT} mice presented higher activity in day time (8:00~20:00), but Foxn1^{L19M} was more active in night time (20:00~08:00) (Figure 5b). Most of all, analysis on oxygen (VO2) and carbon dioxide consumption (VO2) analysis, Foxn1$^{L19M\text{-}HFD}$ exhibited remarkable different pattern with Foxn1$^{WT\text{-}NC}$ in day and night time, and interestingly, VO2 and VCO2 pattern of Foxn1$^{L19M\text{-}HFD}$ was almost similar with that of mice with normal chow. Energy expenditure (EE) was calculated with abbreviated weir formula, and EE pattern showed almost overlapped pattern with that

from normal chow supplied mice, overall EE of Foxn1^{L19M} was lower than Foxn1^{WT}. Respiratory exchange ratio (RER) between Foxn1^{L19M} and Foxn1^{WT} was similar respectively in HFD and NC feeding condition, but Foxn1^{L19M} exhibited significant and lower RER value than Foxn1^{WT}, and this would indicated Foxn1^{L19M} use more fat for energy expenditure than Foxn1^{WT}[47] (Figure 5a and 5b). Briefly, Foxn1^{L19M} used more Taken together, Foxn1^{L19M} mice seemed to use more fat for energy source than Foxn1^{WT}.

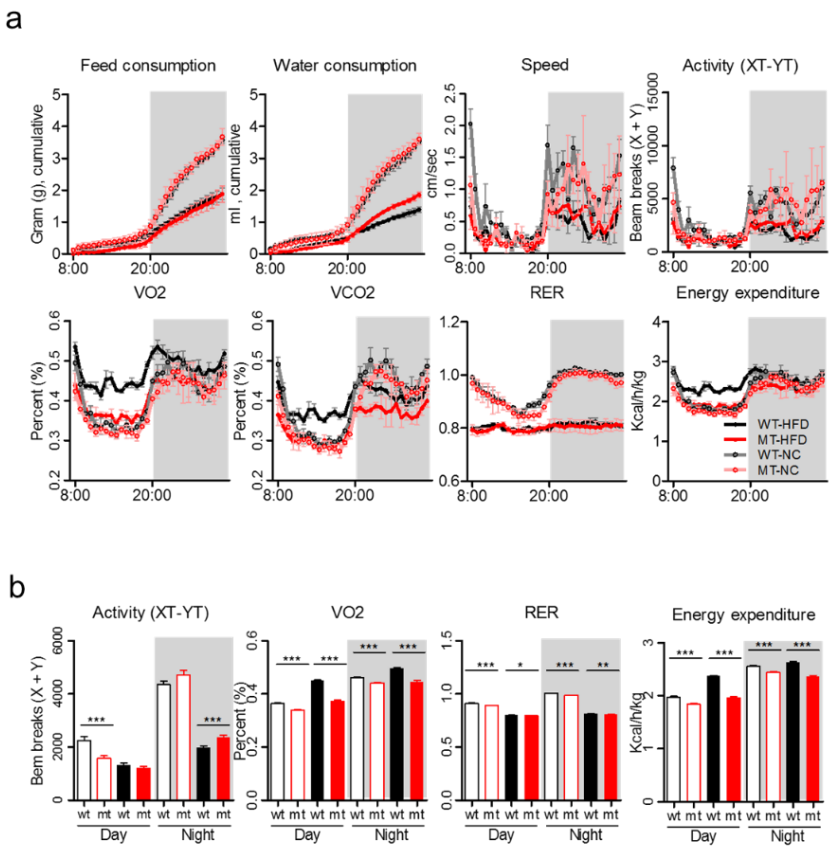

Figure 5. Metabolic phenotype analysis. a. Feed and water consumption, animal movement with speed (cm/sec) and activity (beam break), gas consumption (O_2 and CO_2), respiratory exchange ratio (RER) and abbreviated weir formula derived energy expenditure was measured and analyzed with metabolic cage (n=3 for each group) (Phenomaster). White area: day (08:00~20:00). Gray area: night (20:00~08:00). **b**. Statistical analysis for activity (Beam breaks), gas consumption, RER and energy expenditure depend on day and night for each group. *: $p < 0.05$. ***: $p < 0.0001$ in unpaired student *t* test.

High glucose tolerance with low TG and high HDL in Foxn1^{L19M}

Beige and brown thermogenic fat play role of glucose homeostasis, insulin sensitivity and lipid metabolism, and Foxn1^{L19M} present active subcutaneous fat deposition and more fat for energy source, thus glucose tolerance was assessed with Oral glucose tolerance test (OGTT), insulin tolerance test (ITT) and serum biochemistry. In OGTT, mice with normal chow did not develop difference between mice, but interestingly, Foxn1$^{L19M\text{-}HFD}$ presented high glucose tolerance than Foxn1$^{WT\text{-}HFD}$ (Figure 6a). However, this glucose tolerance in Foxn1^{L19M} did not induced by higher insulin sensitivity (Figure 6b). In further serum chemistry, free fatty acid which cause insulin resistance and inflammation[48], was lower in Foxn1^{L19M}, and triglyceride which is another factor causing insulin resistance exhibited same pattern with FFA. High TG/high density lipoprotein (HDL) ratio are frequently found with persons with insulin resistance[49], but TG/HDL in Foxn1^{L19M} also lower than Foxn1^{WT} (Figure 6c). Even the reason why Foxn1^{L19M} did not exhibit higher insulin sensitivity, but OGTT

and serum chemistry for FFA, TG and HDL suggest high glucose tolerance of

Foxn1^{L19M}

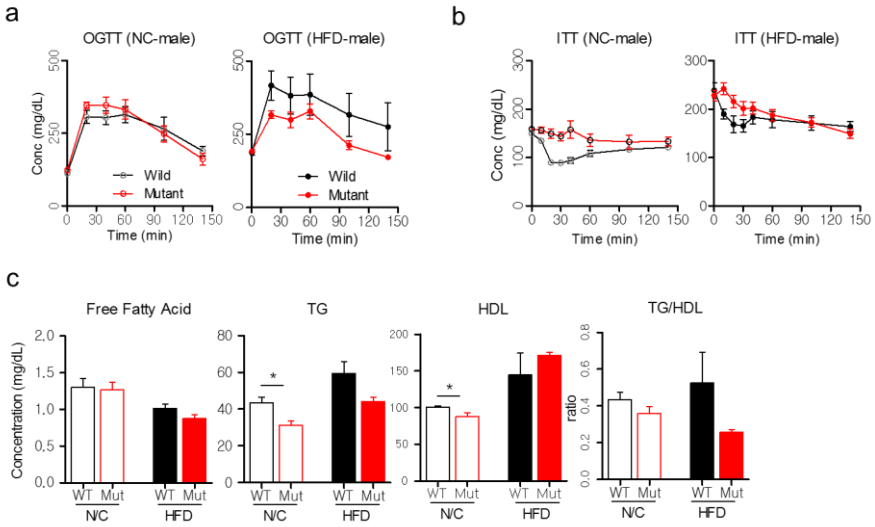

Figure 6. Metabolic phenotype analysis. a. OGTT analysis with Foxn1^{WT} and Foxn1^{L19M}. 1.5 mg/kg glucose injected via per OS route and serum glucose concentrations were measured at 20, 40, 60, 100 and 120 minute after glucose treatment (n/each group: 5), **b**.ITT analysis with 0.5 IU insulin, and serum glucose concentrations were measured after 10, 20, 40, 60 and 100 minute. **c**. Biochemistry for free fatty acid, total glyceride, high density lipoprotein and Tg/HDL ration analysis. *: $p < 0.05$ in unpaired student *t* test (n/each group).

Decreasing Foxn1 expression and upregulation of PPARg and C/EBPa in the mutant mice skin and fat

Since Foxn1 gene expressed in the keratinocyte, so I assume that primary target organ for changing metabolic phenotype would be skin, especially epidermis. Thus, mechanism how Foxn1^{L19M} induced high glucose tolerance was studied in gene expression level. There were many studies for adipogenesis, and PPARg is known as key regulator factor[50], and canonical via wnt10b/β-catenin pathway targeted to PPARg regulation[51]. First total mRNA from skin tissues were extracted and quantitative RT-PCR for Foxn1, Wnt10b, Ctnnb1 and PPARg were conducted. Foxn1^{L19M} seemed to inhibit Foxn1 gene expression, but detail mechanism was not confirmed. Further gene expression analysis for Wnt10b/β-catenin canonical pathway, Foxn1^{L19M} mice exhibited down-regulation of Wnt10b and β-catenin gene in the skin, and this down regulation of Wnt10b/ β-catenin enhanced PPARg upregulation (Figure 7a). These gene expression pattern is consistent with previous report[52]. Additional analysis using iWAT and eWAT, Foxn1 gene expression was not detected but there was

high PPARg expression in Foxn1^{L19M} (Figure 7b). With this results, Foxn1 downregulation induced PPARg upregulation via Wnt10b/ β-catenin pathway. However, I did not confirm the mechanism between Foxn1 and Wnt10b.

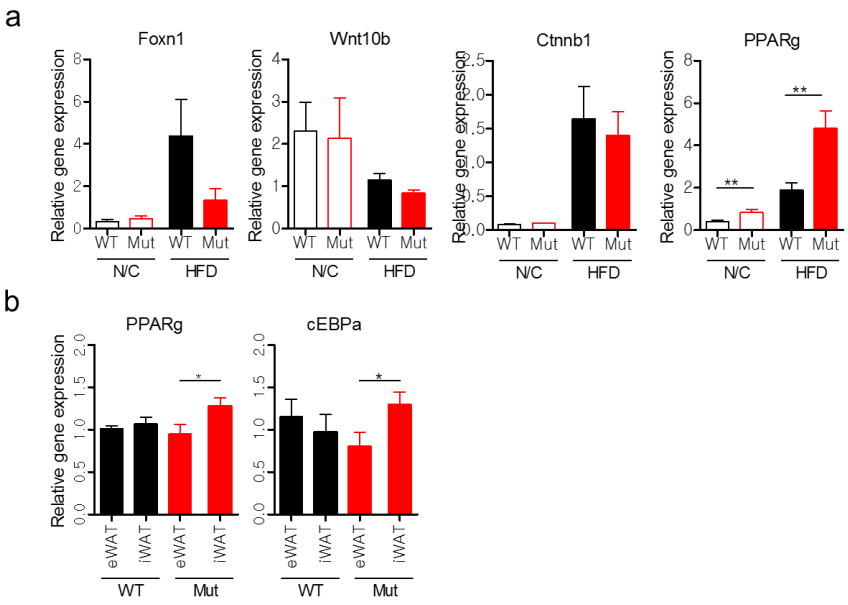

Figure 7. Quantitative RT-PCR for adipogenesis a. qRT-PCR for Foxn1, Wnt10b, Ctnnb1 and PPARg using mRNAs from skin tissues, and gene expression was normalized by that of Actin gene. B. qRT-PCR with mRNAs from iWAT and eWAT, and gene expression was normalized with TBP. *: $p < 0.05$. **: $p < 0.001$ in unpaired student t test.

Discussion

Obesity is increasing of adipocyte tissue mass with hypertrophy and hyperplasia, and is has high correlation with many serious diseases. For several decades, many studies were conduct for studying regulating adipogenesis and its character for metabolic health[53]. In this study, I generated Foxn1 SNP mice with Cas9-BE, and studied metabolic phenotype with produced Foxn1^{L19M} mice. Interestingly, Foxn1^{L19M} mice presented higher adipogenesis in every site of fat with Foxn1 gene inhibition and activation of PPARg, but exhibited good glucose tolerance. With this findings, I suggest that Fox1 is one of regulator for thermogenic epidermal adipogenesis.

First, I used SNP mice for gene function analysis. According to the ClinVar database, many human genetic disorder cause disease, notably SNP with nonsense and missense mutation is dominant[54]. Even gene function studies with loss of function of knock out mouse was well established and discovered many fundamental findings[55], but it

has limitation on studying gene to gene interaction and gene activation/repression. While, mice with SNP would give alternative insight of gene function analysis and new target discovery. Foxn1 KO mice showed hairless and athymic phenotype, so nude mice were popularly used for many studies such as cell transplantation. Recently, Foxn1 gene has spotlight with skin homeostasis and wound healing with MMP family genes[56]. Distinct with previous interesting for Foxn1, I focused on metabolic phenotype causing by Foxn1[56, 57].

Gene expression using Foxn1L19M mice reveal that inhibition of Foxn1 gene in the skin derived PPARg upregulation via Wnt10b/β-catenin pathway. According to GeneCard database (https://www.genecards.org/cgi-bin/carddisp.pl?gene=FOXN1), Foxn1 gene expressed in most type of cell and organ except white blood cells, but the highest expression was observed in the skin tissues, and it might be skin keratinocyte[58]. Stimulation of Foxn1 in keratinocyte is observed in hypoxia or mechanical wound and promoting epithelial to mesenchymal transition[22, 23]. While,

Foxn1 KO mice exhibited upregulation of MMP family and downregulation of BMPs[36]. Even healthy metabolic phenotype in Foxn1^{L19M} was not expected finding, it reveals there might be another mechanism for improving glucose tolerance.

Recently Giacomo et al[46] reported that keratinocyte derived adipogenesis factor stimulate β-catenin activation, and this would have correlation with our finding that foxn1-keratinocyt-Wnt10b/β-catenin axis would regulate epidermal adipogenesis and enhance systemic glucose homeostasis. Actually, there could be other possibilities such as 1) direct interaction of Fox1L19M with PPARg and 2) indirect interaction via immune cell or cytokine to PPARg. However, there was evidence of higher PPARg expression in every examined fat tissues.

Foxn1L19M mice presented good glucose tolerance in OGTT and serum chemistry, but also showed weak insulin sensitivity in ITT analysis. Actually, this is controversial observation as low insulin sensitivity but good insulin tolerance. Even the correct

reason is still unobvious, but high PPARg expression would be answer for good insulin tolerance as similar experiment of PPARg agonist treatment for insulin resistance[59]. In addition, there is still need for measuring insulin concentration and comparing with $Foxn1^{WT}$. Even Foxn1L19M developed good metabolic phenotype with obese phenotype, there is still several limitations. First, in vitro study for elucidating Foxn1 to PPARg mechanism is essential for further study, and second, gene expression was just measured with mRNA level, so confirming with protein level is needed. In conclusion, I generated Foxn1 SNP mice, and presented the possibility of systemic glucose intolerance vial epidermal adipogenesis. With further study for gene interaction between Foxn1 and PPARG, new therapeutic target for metabolic disease could be discovered.

References

1. Islam, N., et al., *The autoimmune basis of alopecia areata: a comprehensive review.* Autoimmun Rev, 2015. **14**(2): p. 81-9.
2. Pratt, C.H., et al., *Alopecia areata.* Nat Rev Dis Primers, 2017. **3**: p. 17011.
3. Dy, L.C. and D.A. Whiting, *Histopathology of alopecia areata, acute and chronic: Why is it important to the clinician?* Dermatol Ther, 2011. **24**(3): p. 369-74.
4. Ito, T., et al., *Maintenance of hair follicle immune privilege is linked to prevention of NK cell attack.* J Invest Dermatol, 2008. **128**(5): p. 1196-206.
5. Gilhar, A., R. Paus, and R.S. Kalish, *Lymphocytes, neuropeptides, and genes involved in alopecia areata.* J Clin Invest, 2007. **117**(8): p. 2019-27.
6. Gilhar, A., et al., *Alopecia areata: Animal models illuminate autoimmune pathogenesis and novel immunotherapeutic strategies.* Autoimmun Rev, 2016. **15**(7): p. 726-35.
7. Nagy, G., et al., *Selected Aspects in the Pathogenesis of Autoimmune Diseases.* Mediators Inflamm, 2015. **2015**: p. 351732.
8. Tembhre, M.K. and V.K. Sharma, *T-helper and regulatory T-cell cytokines in the peripheral blood of patients with active alopecia areata.* Br J Dermatol, 2013. **169**(3): p. 543-8.
9. Shin, B.S., et al., *Impaired inhibitory function of circulating $CD4^+CD25^+$ regulatory T cells in alopecia areata.* J Dermatol Sci, 2013. **70**(2): p. 141-3.
10. Sundberg, J.P., W.R. Cordy, and L.E. King, Jr., *Alopecia areata in aging C3H/HeJ mice.* J Invest Dermatol, 1994. **102**(6): p. 847-56.
11. Zoller, M., et al., *Transient CD44 variant isoform expression and reduction in $CD4(^+)/CD25(^+)$ regulatory T cells in C3H/HeJ mice with alopecia areata.* J Invest Dermatol, 2002. **118**(6): p. 983-92.
12. Salomon, B., et al., *B7/CD28 costimulation is essential for the homeostasis of the $CD4^+CD25^+$ immunoregulatory T cells that control autoimmune diabetes.* Immunity, 2000. **12**(4): p. 431-40.
13. Bielinska, A.U., et al., *Distinct pathways of humoral and cellular immunity induced with the mucosal administration of a nanoemulsion adjuvant.* J Immunol, 2014. **192**(6): p. 2722-33.
14. Zhong, J., et al., *T-cell costimulation protects obesity-induced adipose inflammation and insulin resistance.* Diabetes, 2014. **63**(4): p. 1289-302.
15. Bour-Jordan, H., et al., *Costimulation controls diabetes by altering the balance of pathogenic and regulatory T cells.* J Clin Invest, 2004. **114**(7): p. 979-87.
16. Zeng, M., E. Guinet, and M. Nouri-Shirazi, *B7-1 and B7-2 differentially control peripheral homeostasis of $CD4(^+)CD25(^+)Foxp3(^+)$ regulatory T cells.* Transpl Immunol, 2009. **20**(3): p. 171-9.

17. Alli, R., et al., *A mouse model of clonal CD8$^+$ T lymphocyte-mediated alopecia areata progressing to alopecia universalis.* J Immunol, 2012. **188**(1): p. 477-86.
18. Spandidos, A., et al., *PrimerBank: a resource of human and mouse PCR primer pairs for gene expression detection and quantification.* Nucleic Acids Res, 2010. **38**(Database issue): p. D792-9.
19. Alzolibani, A.A., *Epidemiologic and genetic characteristics of alopecia areata (part 1).* Acta Dermatovenerol Alp Pannonica Adriat, 2011. **20**(4): p. 191-8.
20. Sundberg, J.P., et al., *Animal Models for Alopecia Areata: What and Where?* J Investig Dermatol Symp Proc, 2015. **17**(2): p. 23-6.
21. Sundberg, J.P., et al., *Primary follicular dystrophy with scarring dermatitis in C57BL/6 mouse substrains resembles central centrifugal cicatricial alopecia in humans.* Vet Pathol, 2011. **48**(2): p. 513-24.
22. Ito, T., *Recent advances in the pathogenesis of autoimmune hair loss disease alopecia areata.* Clin Dev Immunol, 2013. **2013**: p. 348546.
23. Muller-Rover, S., et al., *A comprehensive guide for the accurate classification of murine hair follicles in distinct hair cycle stages.* J Invest Dermatol, 2001. **117**(1): p. 3-15.
24. Attridge, K. and L.S. Walker, *Homeostasis and function of regulatory T cells (Tregs) in vivo: lessons from TCR-transgenic Tregs.* Immunol Rev, 2014. **259**(1): p. 23-39.
25. Beyersdorf, N., T. Kerkau, and T. Hunig, *CD28 co-stimulation in T-cell homeostasis: a recent perspective.* Immunotargets Ther, 2015. **4**: p. 111-22.
26. Klein, L., et al., *Positive and negative selection of the T cell repertoire: what thymocytes see (and don't see).* Nat Rev Immunol, 2014. **14**(6): p. 377-91.
27. Nie, J., et al., *FOXP3(+) Treg Cells and Gender Bias in Autoimmune Diseases.* Front Immunol, 2015. **6**: p. 493.
28. Fuse, S., W. Zhang, and E.J. Usherwood, *Control of memory CD8$^+$ T cell differentiation by CD80/CD86-CD28 costimulation and restoration by IL-2 during the recall response.* J Immunol, 2008. **180**(2): p. 1148-57.
29. Dunham, R.M., et al., *CD127 and CD25 expression defines CD4$^+$ T cell subsets that are differentially depleted during HIV infection.* J Immunol, 2008. **180**(8): p. 5582-92.
30. Quinn, K.M., et al., *Inactivation of CD4$^+$ CD25$^+$ regulatory T cells during early mycobacterial infection increases cytokine production but does not affect pathogen load.* Immunol Cell Biol, 2006. **84**(5): p. 467-74.
31. Garg, S.K., et al., *Aging is associated with increased regulatory T-cell function.* Aging Cell, 2014. **13**(3): p. 441-8.
32. Stern, J.H. and P.E. Scherer, *Adipose tissue biology in 2014: Advances in our understanding of adipose tissue homeostasis.* Nat Rev Endocrinol, 2015. **11**(2): p. 71-2.
33. Gesta, S., Y.H. Tseng, and C.R. Kahn, *Developmental origin of fat: tracking obesity to its source.* Cell, 2007. **131**(2): p. 242-56.

34. Masuzaki, H., et al., *A transgenic model of visceral obesity and the metabolic syndrome.* Science, 2001. **294**(5549): p. 2166-70.
35. Palamaro, L., et al., *FOXN1 in organ development and human diseases.* Int Rev Immunol, 2014. **33**(2): p. 83-93.
36. Kur-Piotrowska, A., et al., *Neotenic phenomenon in gene expression in the skin of Foxn1- deficient (nude) mice - a projection for regenerative skin wound healing.* BMC Genomics, 2017. **18**(1): p. 56.
37. Stemmer, K., et al., *Thermoneutral housing is a critical factor for immune function and diet-induced obesity in C57BL/6 nude mice.* Int J Obes (Lond), 2015. **39**(5): p. 791-7.
38. Shastry, B.S., *SNPs: impact on gene function and phenotype.* Methods Mol Biol, 2009. **578**: p. 3-22.
39. Grabowska, A.I. and T. Wilanowski, *FOXN1 Transcription Factor in Epithelial Growth and Wound Healing.* Mol Cell Biol, 2017. **37**(17).
40. Nakagawa, S., et al., *DNA-binding specificity changes in the evolution of forkhead transcription factors.* Proc Natl Acad Sci U S A, 2013. **110**(30): p. 12349-54.
41. View ORCID ProfileJoseph A. Newman, H.A., Angeline Gravard, Ioanna A. Rota, Adam E. Handel, View ORCID ProfileGeorg A. Hollander, View ORCID ProfileOpher Gileadi, *The structural basis for forkhead box family specificity revealed by the crystal structure of human FOXN1 in complex with DNA.* BioRxiv, 2018.
42. Marx, V., *Base editing a CRISPR way.* Nat Methods, 2018. **15**(10): p. 767-770.
43. Dakin, R.S., et al., *Estrogens protect male mice from obesity complications and influence glucocorticoid metabolism.* Int J Obes (Lond), 2015. **39**(10): p. 1539-47.
44. Murano, I., et al., *Dead adipocytes, detected as crown-like structures, are prevalent in visceral fat depots of genetically obese mice.* J Lipid Res, 2008. **49**(7): p. 1562-8.
45. Wu, J., et al., *Beige adipocytes are a distinct type of thermogenic fat cell in mouse and human.* Cell, 2012. **150**(2): p. 366-76.
46. Donati, G., et al., *Epidermal Wnt/beta-catenin signaling regulates adipocyte differentiation via secretion of adipogenic factors.* Proc Natl Acad Sci U S A, 2014. **111**(15): p. E1501-9.
47. Lou, P.H., et al., *Increased lipolysis and energy expenditure in a mouse model with severely impaired glucagon secretion.* PLoS One, 2011. **6**(10): p. e26671.
48. Boden, G., *Obesity and free fatty acids.* Endocrinol Metab Clin North Am, 2008. **37**(3): p. 635-46, viii-ix.
49. da Luz, P.L., et al., *High ratio of triglycerides to HDL-cholesterol predicts extensive coronary disease.* Clinics (Sao Paulo), 2008. **63**(4): p. 427-32.
50. Lefterova, M.I., et al., *PPARgamma and the global map of adipogenesis and beyond.* Trends Endocrinol Metab, 2014. **25**(6): p. 293-302.
51. Vallee, A. and Y. Lecarpentier, *Crosstalk Between Peroxisome Proliferator-Activated Receptor Gamma and the Canonical WNT/beta-Catenin Pathway in Chronic*

Inflammation and Oxidative Stress During Carcinogenesis. Front Immunol, 2018. **9**: p. 745.

52. Ackers, I. and R. Malgor, *Interrelationship of canonical and non-canonical Wnt signalling pathways in chronic metabolic diseases.* Diab Vasc Dis Res, 2018. **15**(1): p. 3-13.
53. Ghaben, A.L. and P.E. Scherer, *Adipogenesis and metabolic health.* Nat Rev Mol Cell Biol, 2019. **20**(4): p. 242-258.
54. Landrum, M.J., et al., *ClinVar: public archive of interpretations of clinically relevant variants.* Nucleic Acids Res, 2016. **44**(D1): p. D862-8.
55. Brown, S.D. and M.W. Moore, *The International Mouse Phenotyping Consortium: past and future perspectives on mouse phenotyping.* Mamm Genome, 2012. **23**(9-10): p. 632-40.
56. Bukowska, J., et al., *Foxn1 in Skin Development, Homeostasis and Wound Healing.* Int J Mol Sci, 2018. **19**(7).
57. Kur-Piotrowska, A., et al., *Foxn1 expression in keratinocytes is stimulated by hypoxia: further evidence of its role in skin wound healing.* Sci Rep, 2018. **8**(1): p. 5425.
58. Janes, S.M., et al., *Transient activation of FOXN1 in keratinocytes induces a transcriptional programme that promotes terminal differentiation: contrasting roles of FOXN1 and Akt.* J Cell Sci, 2004. **117**(Pt 18): p. 4157-68.
59. Choi, S.S., et al., *PPARgamma Antagonist Gleevec Improves Insulin Sensitivity and Promotes the Browning of White Adipose Tissue.* Diabetes, 2016. **65**(4): p. 829-39.

국문초록

피부는 부상과 감염에서 신체를 보호하는 첫번째 장벽으로, 기관 중 표면적이 가장 큰 장기 중 하나입니다. 특히 단순한 물리적 장벽으로만 여겨지던 과거와는 달리 최근의 연구들은 피부가 신체의 항상성을 보장하는 최전선의 기관으로 면역 또는 비면역과 관련된 인체의 건강에 능동적으로 기여하는 바를 강조하고 있습니다. 이러한 기능의 수행을 이해하기 위해서는 피부를 구성하는 각 하위 집단 간의 상호 작용과 그 결과에 대한 관찰이 필요합니다.

대게 세포들의 단편적인 기능 연구는 그와 관련된 유전자를 변형시키는 것만으로도 관찰할 수 있지만, 앞서 언급된 것처럼 다양한 세포 집단으로 구성되는 피부는 상호 간의 네트워크가 중요한 장기입니다. 따라서, In Vitro 연구만으로는 부족할 수 있는 상호 작용의 결과는 유전자 변형 동물 모델을 통하여 실제와 유사한 환경에서의 표현형을 관찰하는 것이 유리합니다.

이 연구에서는 CD80CD86 유전자 변형을 통한 피부에서의 면역과 관련된 연구 및 Foxn1 유전자 변형을 통한 신진 대사 변화를 관찰하였습니다. 효율적이고 비교적 간단한 게놈 편집

도구로 확인된 CRISPR/Cas system 을 이용하여 형질 전환 마우스를 제작하였으며, 표현형 분석을 진행하였습니다.

본 연구에서 가장 중요한 점은 복잡하고 다양한 피부의 구성과 기능을 복합적으로 고려하여 표현형을 분석함으로써 실제와 최대한 유사한 결과를 도출할 수 있음을 보여준 것입니다.

결론적으로, 이 연구는 단일 유전자의 변형을 통하여 피부에서의 자가면역질환과 관련된 탈모 및 표피와 관련된 신진대사 변화의 표현형을 발견하였습니다.